PNAS RESEARCH ARTICLE | CELL BIOLOGY OPEN ACCESS

# OGG1S326C variant frequent in human populations facilitates inflammatory responses due to its extended interaction with DNA substrate

Jinling Han[a,b], Meichen Zhang[a,b], Jiakun Ge[a,b], Zhihua Ji[a,b], Jianyi Zhao[c], Yinchao Hu[a,b], Chunshuang Li[a,b], Yaoyao Xue[a,b], Xining Li[a,b], Haiwang Zhao[a,b], Zixu Cui[a,b], Miaomiao Tian[a,b], Xu Zheng[a,b], Dapeng Wang[d], Jing Wang[c], Min Wei[a,b], Zsolt Radak[e], Yusaku Nakabeppu[f], Istvan Boldogh[g], and Xueqing Ba[a,b,1]

Affiliations are included on p. 12.

Edited by Andre Nussenzweig, National Cancer Institute, Bethesda, MD; received February 23, 2025; accepted March 21, 2025

**8-oxoguanine (8-oxoGua) is one of the most frequent forms of oxidative DNA base lesions, repaired by 8-oxoguanine DNA glycosylase 1 (OGG1) via base excision repair (BER) pathway to maintain genome fidelity. The human allelic variant *hOGG1*$^{S326C}$, prevalent in Caucasians and Asians, has been regarded as a susceptibility factor for various diseases, yet its pathogenic mechanism remains elusive. In this study, we demonstrate that *Ogg1*$^{S326C/S326C}$ mice exhibit increased and sustained airway inflammation compared with wild-type (WT) *Ogg1*$^{S326/S326}$ mice. Mechanistically, in response to inflammatory stimulation, OGG1S326C undergoes reactive oxygen species-induced dimerization, which impairs its base excision function, but prolongs its association with promoter-embedded substrate(s), leading to an increase in NF-κB' DNA occupancy, subsequently the excessive expression of proinflammatory cytokines and chemokines, and the exacerbated lung inflammation. In contrast, Serine at position 326 in WT -OGG1 is constitutively phosphorylated by CDK4. To fulfill the requirement for its function in transcriptional regulation, the phosphorylated OGG1 needs to undergo dephosphorylation to rescue DNA binding ability. In this scenario, OGG1S326C lacks this phosphorylation site, disrupting this regulatory cycle. Notably, administration of a small molecule inhibitor of OGG1 prevents OGG1S326C from binding to DNA and significantly decreases gene expression and inflammatory responses. Our findings elucidate a molecular basis for the increased disease susceptibility of individuals carrying the *hOGG1*$^{S326C}$ variant and propose the therapeutic potential of OGG1 inhibitors in mitigating inflammation-driven pathologies.**

8-oxoguanine DNA glycosylase-1 (OGG1) | OGG1S326C | single nucleotide polymorphism | inflammatory gene expression | lung injury

## Significance

OGG1S326C, a variant widely recognized as a risk factor for various malignancies and other diseases, has drawn significant attention due to its high prevalence (~20% in Caucasians and ~40 to 60% in Asians) in human populations. Despite its reduced DNA repair activity, individuals carrying this variant do not exhibit 8-oxoGua accumulation in their genomes, suggesting that the association between the *OGG1*$^{S326C}$ genotype and disease susceptibility involves mechanisms beyond the mutagenic effects of 8-oxoGua. In this study, we identify a molecular mechanism by which the OGG1S326C variant drives excessive expression of proinflammatory cytokines and chemokines, contributing to various inflammation-related diseases in humans.

Reactive oxygen species (ROS), which are generated either through endogenous metabolism or in response to environmental challenges, can instigate oxidative damage to DNA (1). Among DNA bases, guanine has the lowest redox potential and is particularly susceptible to being oxidized by ROS to generate base lesion 8-oxo-7, 8-dihydroguanine (8-oxoGua). 8-OxoGua is commonly regarded as a biomarker of oxidative stress and is repaired through 8-oxoguanine DNA glycosylase 1 (OGG1)-initiated base excision repair (BER) pathway (2, 3). If left unrepaired, 8-oxoGua may pair with cytosine (Cyt) in trans or with adenine (Ade) *in syn* during DNA replication, potentially leading to a G:C to T:A transversion mutation after two rounds of cell cycles (4, 5). The accumulation of 8-oxoGua in the genome is frequently associated with various aging-related diseases including cancers and neurodegenerative disorders. Consequently, the single nucleotide polymorphisms (SNPs) in human *OGG1* gene (*hOGG1*), and their effects on the repair activity of hOGG1 have captured increasing attention in the field of genomic stability and disease research.

To date, at least 20 SNPs of *hOGG1* have been reported. Among them, the most conspicuous one is *hOGG1*$^{S326C}$ due to its high frequency in the human population. This SNP occurs in the seventh exon of *hOGG1*, where the Cyt at position 1245 is mutated to guanine (Gua), resulting in a serine to cysteine substitution at site 326 of hOGG1 (6). Epidemiological studies have revealed that the frequency of this SNP is about 20% in Caucasian populations, but as high as 40 to 60% in Asian populations (7, 8). Epidemiological case–control cohort studies have suggested that *hOGG1*$^{S326C}$ is a risk factor for a variety of inflammatory and metabolic diseases, as well as cancers, such as lung cancer (9), gastric cancer (10), prostatic cancer (11), oropharyngeal cancer (12), as well as diabetes (13), Alzheimer's disease (14), and chronic obstructive pulmonary disease (COPD) (15).

Analyses of the efficiency of hOGG1 in 8-oxoGua repair revealed a compromised enzymatic activity of hOGG1S326C (16, 17); however, cells from *hOGG1*$^{S326C}$ individuals did not show an accumulation of more 8-oxoGua in DNA compared with the cells from individuals expressing hOGG1S326. More importantly (6, 7), the genotype of *hOGG1*$^{S326C}$ was not found to be associated with genome instability of the human genome (18). Therefore, the direct

Author contributions: J.H., X.B., M.W., Z.R., Y.N., and I.B. designed research; J.H., M.Z., J.G., Z.J., J.Z., Y.H., C.L., Y.X., X.L., H.Z., Z.C., M.T., X.Z., D.W., and J.W. performed research; J.H., D.W., and Y.N. contributed new reagents/analytic tools; J.H. and M.Z. analyzed data; and J.H., X.B., and I.B. wrote the paper.

The authors declare no competing interest.

This article is a PNAS Direct Submission.



[1]To whom correspondence may be addressed. Email: baxq755@nenu.edu.cn.

This article contains supporting information online at https://www.pnas.org/lookup/suppl/doi:10.1073/pnas.2426102122/-/DCSupplemental.

Published May 9, 2025.

etiological evidence linking the *hOGG1*$^{S326C}$ variation with disease susceptibility is still missing.

Recent studies have revealed a novel mechanism by which OGG1 contributes to the transcriptional activation of pro-inflammatory cytokines/chemokines. The promoter regions of these genes are typically GC-rich. Oxidative stress generates 8-oxoGua in inflammatory gene promoters, and also results in a transient enzymatic inactivation of OGG1 (19–21). In this scenario, OGG1 binds to the substrate in gene regulatory sequences without promptly performing base excision. Instead, it acts as a scaffold, recruiting transcription factors including NF-κB and other components of transcription machinery to facilitate the timely expression of ROS-responsive inflammatory genes (19, 22–24).

In this study, we propose that the increased disease susceptibility of individuals expressing hOGG1S326C stems from its compromised lesion excision activity, which likely increases inflammation-driven pathologies. To test this hypothesis, we generated mice with the *Ogg1*$^{S326C/S326C}$ and *Ogg1*$^{S326/S326}$ genotypes, as well as cells expressing hOGG1S326C and phosphor-mimetic WT -OGG1 mutants, and employed histological, cellular, molecular, and biochemical assays to define the underlying mechanism. Our findings demonstrate that substituting serine (Ser) with cysteine (Cys) at position 326 in WT -OGG1, disrupts regulation by CDK4-driven phosphorylation, promoting dimerization, prolonged the association with DNA substrate(s), increases DNA occupancy of transcription factors, consequently enhances the expression of cytokines and chemokines and the immunopathology in a mouse model. Importantly, the OGG1 inhibitor significantly reduced both OGG1 and OGG1S326C substrate binding, dampened the transcriptional activation and alleviated lung inflammation. These results not only elucidate the underlying mechanism, but also highlight a promising clinical strategy for managing inflammation-related diseases in individuals carrying the hOGG1S326C variant.

## Results

**The OGG1S326C Variant Induces Prolonged Expression of Proinflammatory Cytokines/Chemokines.** Given the close correlation between the *hOGG1*$^{S326C}$ genotype and the development of lung diseases (25), we established an acute lung injury model using C57BL/6 J mice by intranasally (i.n.) challenging with lipopolysaccharide (LPS) to induce proinflammatory gene expression with or without a prior intraperitoneal (i.p.) administration of TH5487, a potent and specific active site inhibitor, to prevent OGG1 from binding to its DNA substrate (26). Lungs were collected at 0, 2, 16, and 24 h post LPS challenge. The mRNA levels of proinflammatory cytokine and chemokine were examined by RT-qPCR. The results showed a robust expression of multiple proinflammatory cytokines and chemokines and confirmed the importance of OGG1 binding to genomic substrates for the gene expression (Fig. 1*A* and *SI Appendix*, Fig. S1*A*). The protein level of OGG1 showed no change throughout the inflammation with or without treatment with TH5487 (*SI Appendix*, Fig. S1*B*).

To investigate the impact of the human (*h)OGG1*$^{S326C}$ genotype in inflammatory gene expression, *Ogg1*$^{S326/S326}$ and *Ogg1*$^{S326C/S326C}$ mice were generated using CRISPR-Cas9 gene-editing technology. The sequences coding for amino acid residues 326~330 were either replaced to SRHAQ in *Ogg1*$^{S326/S326}$, or to CRHAQ in *Ogg1*$^{S326C/S326C}$ from PSLSR in *Ogg1*$^{+/+}$ allele to create the identical sequence contexts of site 326 of *hOGG1* (Fig. 1*B*). Genotypes of the genetically engineered mice were confirmed by sequencing. The replacement of the amino acid residues does not change OGG1's expression as determined at both mRNA and protein levels (*SI Appendix*, Fig. S1 *C* and *D*). To assess the expression of proinflammatory genes in the lungs of mice with *Ogg1*$^{S326/S326}$, *Ogg1*$^{S326C/S326C}$, *Ogg1*$^{+/+}$, and *Ogg1*$^{-/-}$ genotypes, a 2 h time point was chosen. The results revealed a significantly higher expression of *Cxcl2*, *Cxcl1*, *Ccl2*, *Ccl20*, *Il6,* and *Tnf-α* in mice with *Ogg1*$^{S326C/S326C}$ genotype compared with that in mice with *Ogg1*$^{S326/S326}$ genotype in this acute lung injury model. Conversely, the expression levels of the above genes in *Ogg1*$^{-/-}$ mice were lower than those in mice with *Ogg1*$^{+/+}$ genotype. Notably, except in *Ogg1*$^{-/-}$ mice, the OGG1 inhibitor TH5487 effectively inhibited the expression of proinflammatory genes in all mice including those with *Ogg1*$^{S326C/S326C}$ genotype (Fig. 1 *C–E*). After 16-h LPS challenge, the lung tissues from mice with different genotypes were subjected to H&E staining and pathological examinations (Fig. 2 *A–D* and *SI Appendix*, Fig. S2*A*). In parallel, bronchoalveolar lavage fluid (BALF) analysis was performed. The results showed that the *Ogg1*$^{S326C/S326C}$ mice exhibited higher level of inflammatory cell infiltration, with the number of neutrophils significantly increased (>18 × $10^4$ cells/mL) in the BALF compared with that of *Ogg1*$^{S326/S326}$ mice, where the count reached >15× $10^4$ cells/mL. Additionally, the level of inflammatory cell infiltration in lung tissues and the neutrophils in the BALF of *Ogg1*$^{+/+}$ mice were higher than those observed in the lungs of *Ogg1*$^{-/-}$ mice. Notably, in *Ogg1*$^{S326C/S326C}$ mice, treatment with an OGG1 inhibitor significantly lowered the inflammatory cell infiltration, decreased the number of neutrophils in the BALF, and maintained the integrity of lung tissue (Fig. 2 *E–H* and *SI Appendix*, Fig. S2*B*).

Moreover, mouse embryonic fibroblast (MEF) cells with or without *Ogg1* expression were used. In response to TNFα exposure, the expression of inflammatory genes in *Ogg1*$^{-/-}$ cells was significantly lower compared with that in *Ogg1*$^{+/+}$ cells (Fig. 3*A*). Subsequently, ectopic expression of WT -hOGG1 (YFP-OGG1) and its variants (YFP-OGG1S326C, YFP-OGG1F319A) was achieved in *Ogg1*$^{-/-}$ MEF cells. OGG1F319A was used as a negative control, which no longer engages with 8-oxoGua but retains the ability to interact with DNA (27, 28). Upon TNFα stimulation, the expression of *Cxcl2*, *Cxcl1*, *Tnf-α,* and *Il6* in cells expressing WT -OGG1 increased within the first 30 min, peaked at 1 h, and significantly decreased at 2 h. Importantly, the expression of these genes in cells expressing OGG1S326C was not only higher than that in wt-OGG1-expressing cells at 30 min and 1 h, but also remained elevated at 2 h, indicating the OGG1S326C variant promotes sustained upregulation of gene transcription. As a control, cells expressing OGG1F319A that lacks substrate binding ability did not show a significant increase in the expression of the tested genes (Fig. 3*B* and *SI Appendix*, Fig. S3). Furthermore, an RNA-FISH assay revealed that upon inflammatory stimulation, *Cxcl2* expression in cells with ectopic expression of OGG1S326C was higher than that in cells transfected with the plasmid expressing WT -OGG1. In contrast, *Cxcl2* expression was barely detectable in cells expressing OGG1F319A (Fig. 3 *C* and *D*).

**The Association of OGG1S326C with DNA Substrate Increases in Parallel with its Decreased Enzymatic Activity.** To investigate whether the increased transcriptional activity of OGG1S326C correlates with its impaired activity to remove 8-oxoGua from genome upon oxidative stress, mice with different genotypes were challenged with LPS (10 mg/kg) via nasal route. Two hours later, the lung tissues were digested into single cell suspensions using collagenase, and cells were embedded into agarose and incubated with or without purified recombinant hOGG1 in situ, Fragment Length Analysis using Repair Enzymes (FLARE) comet assay was performed. The results showed that after LPS stimulation, the Olive Tail Moment (OTM) value of cells from the mice with *Ogg1*$^{S326C/S326C}$ genotype was significantly higher than that from the mice with *Ogg1*$^{S326/S326}$ genotype (Fig. 4 *A* and *B*). After saline challenge, the OTM values of the lung tissue cells from both genotypes were low and showed no significant difference. Furthermore, the OTM values of the cells from the mice with *Ogg1*$^{S326/S326}$ and *Ogg1*$^{S326C/S326C}$ genotypes were enhanced upon TH5487 treatment with no significant difference between them. Conversely, in additional control experiments, the FLARE OTM value of lung cells from *Ogg1*$^{+/+}$ mice was significantly lower than that from the *Ogg1*$^{-/-}$ mice (Fig. 4 *C* and *D*). These data suggested that the OGG1S326C variant has a lower ability to timely excise 8-oxoGua from the genome compared with WT -OGG1 under inflammatory conditions.

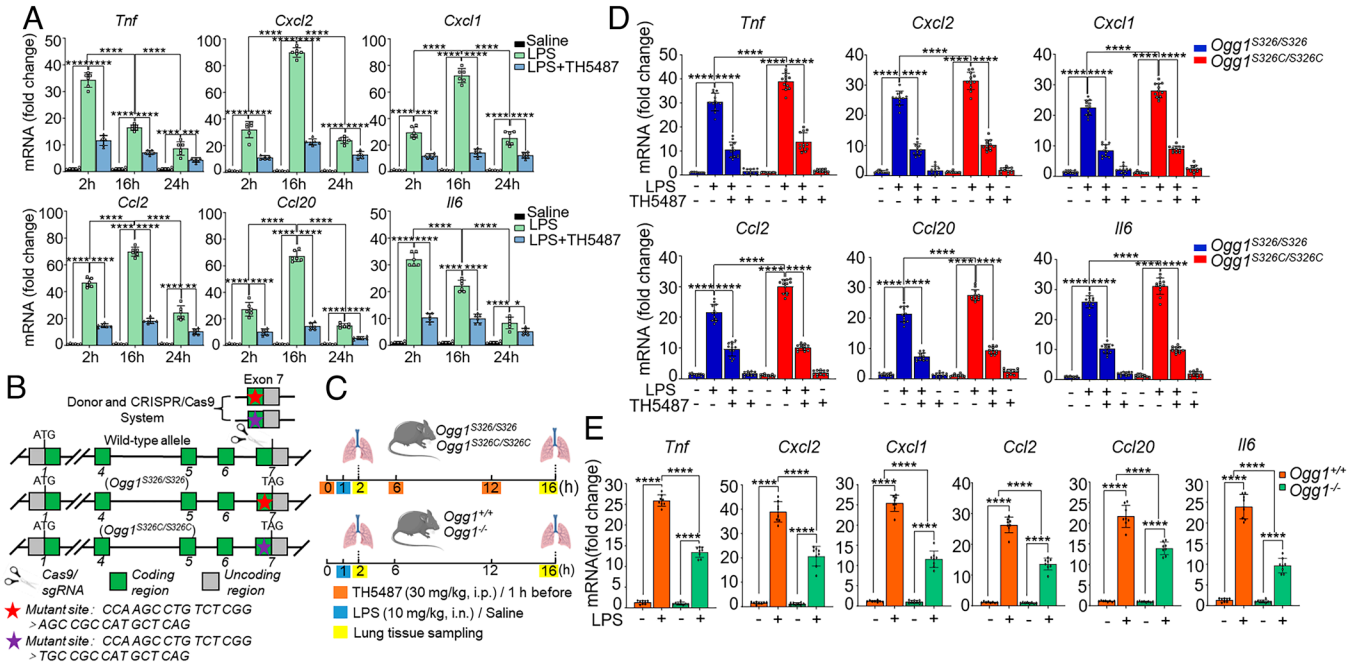


**Fig. 1.** Expression of inflammatory genes is higher in *Ogg1*$^{S326C/S326C}$ mice compared with that in *Ogg1*$^{S326/S326}$ ones. (*A*) Time course of proinflammatory gene expression in response to LPS challenge. Lungs of C57BL/6JGpt mice were challenged with LPS (10 mg/kg) via intranasal route with or without prior intraperitoneal injection of TH5487 (30 mg/kg). Mice obtained physiological saline solution served as control. Lungs were collected at 2, 16, and 24 h post of LPS exposure. Expression of proinflammatory cytokines and chemokines was determined by RT-qPCR. (control group n = 3, experimental group n = 4). (*B*) Diagrams show development of *Ogg1*$^{S326/S326}$ and *Ogg1*$^{S326C/S326C}$ mice using CRISPR/Cas9 system. (*C*) The diagram depicts the schematics for inducing acute lung injury in mice. (*D*) Proinflammatory gene expression is higher in *Ogg1*$^{S326C/S326C}$ mice compared with that in *Ogg1*$^{S326/S326}$ ones. Lungs of *Ogg1*$^{S326/S326}$ and *Ogg1*$^{S326C/S326C}$ mice were challenged with LPS (10 mg/kg) intranasally, with or without prior intraperitoneal administration of TH5487 (30 mg/kg). Two hours post challenge, the expression of selected genes was determined by RT-qPCR. (n = 12, 50% female, 50% male) (*E*) Decreased proinflammatory gene expression in *Ogg1*$^{-/-}$ mice compared with that in *Ogg1*$^{+/+}$ ones. Groups of mice were challenged as described in legend to E, without treatment of OGG1 inhibitor TH5487, and gene expression at mRNA levels was determined by RT-qPCR. (n = 8, 50% female, 50% male). In (*A*), (*D*), and (*E*), A one-way ANOVA of variance was used to indicate the significance of the difference. Data are derived from three independent experiments and are presented as mean ± SEM. **P* < 0.05, ***P* < 0.01, ****P* < 0.001, *****P* < 0.001, ns: not significant.

OGG1 plays an important role in regulating the transcription from pro-inflammatory cytokine/chemokine genes, which is associated with ROS and involves the transiently impaired enzymatic activity of OGG1 for DNA damage repair (19, 20, 24). To further explore this characteristic with OGG1 variants, 8-oxoGua-containing DNA duplex probe with a sequence derived from *Cxcl2* was utilized for cleavage assays and EMSA experiments (*SI Appendix,* Table S1). The activity of GST-OGG1S326C in excising 8-oxoGua from DNA duplex was indeed lower than that of WT -OGG1 as well-known; however, its ability to engage with 8-oxoGua was significantly increased. The dissociation constant ($K_d$) of WT-OGG1' was 1.680, whereas that of OGG1S326C decreased to 0.958, indicating an approximately 50% increase in DNA binding affinity. These differences were confirmed through two-way ANOVA (Fig. 4 *E* and *F* and *SI Appendix*, Fig. S4 *E* and *F*). Notably, the OGG1 inhibitor TH5487 effectively prevented both DNA binding and substrate cleavage of OGG1S326C (Fig. 4 *G* and *H* and *SI Appendix,* Fig. S4 *G* and *H*). As a control, GST-OGG1F319A showed no ability to bind with or to cleave the substrate. GST alone was also incapable of binding with or cleaving the probe (*SI Appendix*, Fig. S4 *A–D*). The results suggested that the enhanced transcriptional activity of OGG1S326C may rely on its sustained binding with intrahelical 8-oxoGua despite its compromised repair function.

It has been documented that OGG1S326C is prone to intermolecular dimerization (29, 30), and has a compromised enzymatic activity for removing 8-oxoGua, thereby posing a risk of mutagenesis and disease for *OGG1*$^{S326C}$ carriers (29, 31). In the present study, cells were cotransfected with plasmids expressing Flag- and YFP-tagged WT -OGG1, or Flag- and YFP-tagged OGG1S326C, and then exposed to TNFα. Proximity ligation assay (PLA) was performed after treatment of cells with cytoskeleton (CSK) buffer. We first demonstrated that in TNFα-exposed cells, there was an increased level of OGG1S326C dimerization within nonsoluble chromatin fraction; however, which was dampened by NAC pretreatment, implying that binding OGG1S326C with its substrate(s) and its dimerization are ROS dependent. (Fig. 5 *A–C* and *SI Appendix*, Fig. S5 *A–C*). Next, we performed fluorescence resonance energy transfer (FRET) acceptor photobleaching analysis. HeLa cells were cotransfected with plasmids expressing donor CFP-WT -OGG1 and acceptor YFP-WT-OGG1, or donor CFP-OGG1S326C and acceptor YFP-OGG1S326C, and then exposed to TNFα. As a positive control, fused CFP-YFP protein was used to show the occurrence of FRET. The results showed that while WT -OGG1 poorly underwent intermolecular interaction upon TNFα exposure, interaction between OGG1S326C molecules was highly significant. (Fig. 5 *A–C*, *D*, and *F* and *SI Appendix*, Fig. S5 *A–C*, *D*, and *F*). In the presence of NAC, the dimerization of OGG1S326C was almost completely diminished (*SI Appendix*, Fig. S5 *D–F*). Taken together, these data suggested ROS-elicited dimerization of OGG1S326C enhances and sustains its engagement with its substrate in nonsoluble chromatin fraction.

**OGG1S326C Sustains DNA Occupancy of NF-κB on Gene Promoters.** To gain insight into why OGG1S326C is more potent in promoting proinflammatory gene expression compared with WT -OGG1, we investigated its ability to bind to promoters and its impact on NF-κB' DNA occupancy. Flag-tagged WT-OGG1, Flag-OGG1S326C, and Flag-OGG1F319A were overexpressed in HEK293 cells respectively. ChIP assays were performed to assess the binding of WT-OGG1 and OGG1S326C to the promoters of the proinflammatory genes. The results showed that, after 60 min TNFα stimulation, the association of OGG1S326C with the promoter regions of *CXCL2, CXCL1, IL6, and TNF-α* significantly increased, compared with that of WT-OGG1. At 120 min, the binding of OGG1S326C in the promoter still remained at a high level. OGG1F319A showed low level (if any) binding to the promoter regions throughout TNFα stimulation (Fig. 6*A*) Nevertheless, TH5487 and NAC decreased the binding of both WT-OGG1 and

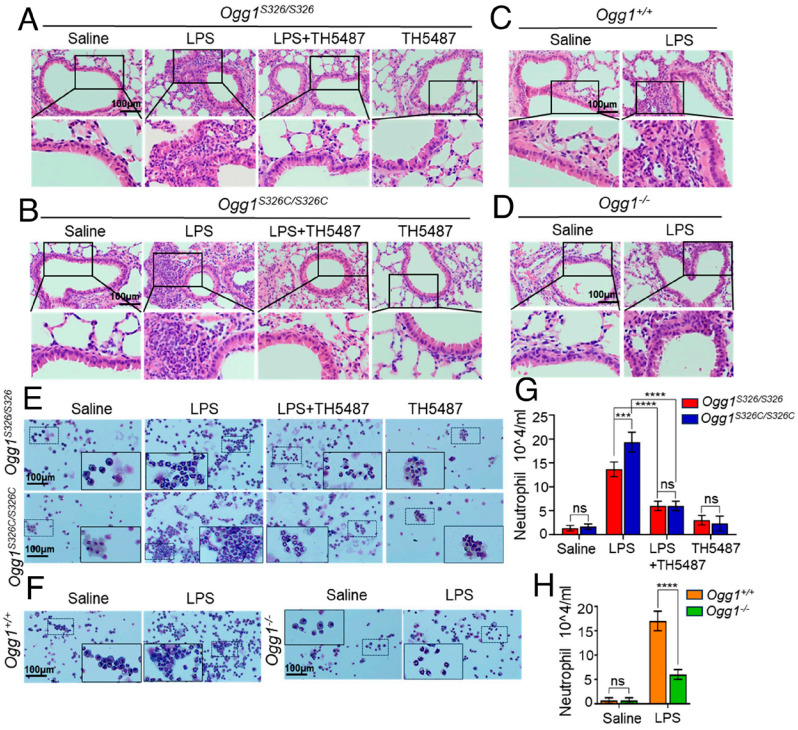


**Fig. 2.** Increased infiltration of inflammatory cells in the lungs of *Ogg1*$^{S326C/S326C}$ mice compared with that of *Ogg1*$^{S326/S326}$ ones. (*A-D*) H&E staining of lung tissue sections to assess the accumulation of inflammation. *Ogg1*$^{S326/S326}$ and *Ogg1*$^{S326C/S326C}$ mice were pretreated intraperitoneally with TH5487 (30 mg/kg) or vehicle. One hour later, the lungs were challenged with LPS (10 mg/kg) via intranasal route for 16 h (*A* and *B*). As a control, *Ogg1*$^{+/+}$ and *Ogg1*$^{-/-}$ mice were exposed to LPS (10 mg/kg) intranasally for 16 h (*C* and *D*). H&E staining showed inflammatory cell infiltration in the peri-bronchial areas. (Scale bar, 100 μm.) (*E-H*) Visual representation of leukocytes in BALF derived from airways. *Ogg1*$^{S326/S326}$, *Ogg1*$^{S326C/S326C}$, *Ogg1*$^{+/+}$, and *Ogg1*$^{-/-}$ mice were treated as described above. BALFs were processed as described in *Materials and Methods*. (Scale bar, 100 μm.) Results represent four independent experiments (*E* and *F*). The average neutrophil count of saline-treated controls in each experiment was set to 1. The data are presented as the mean ± SEM. A one-way ANOVA was used to determine statistical significance (*G* and *H*). $^{**}P < 0.01$, $^{****}P < 0.001$ ns: not significant. Abbreviations: BALF, bronchoalveolar lavage fluid.

OGG1S326C to gene promoters without affecting the expression of OGG1 at the protein level (Fig. 6*B* and *SI Appendix*, Fig. S6 *A* and *B*). Next, the influence of WT-OGG1, OGG1S326C, and OGG1F319A on promoter homing of NF-κB was examined. The result showed that the binding of NF-κB to the promoters of inflammatory genes was significantly higher in OGG1S326C-expressing cells than in WT-OGG1- or OGG1F319A-expressing cells (Fig. 6 *C* and *D*), indicating the distinct effect of OGG1S326C variant on DNA occupancy of NF-κB. Additionally, PLA experiment was performed, and the result showed that OGG1S326C had a significantly higher ability to interact with chromatin-associated RelA/p65 than wt-OGG1 following 60 min TNFα exposure. Treatment with NAC or TH5487 inhibited the association of WT-OGG1 or OGG1S326C with RelA/p65 (Fig. 6 *E–G*). Taken together, the data indicate that OGG1S326C has a greater ability to promote NF-κB binding to gene promoters than WT-OGG1.

**The CDK4-Mediated Phosphorylation of hOGG1 at S326 Declines in Response to Inflammatory Stimulation.** Early studies reported that various protein kinases interact with OGG1 *in vitro;* however, the specific kinase(s) and precise phosphorylation site(s) in vivo had not been identified (32–34). If S326 of hOGG1 is phosphorylated, the introduction of negative charge(s) would impact the binding of OGG1 to DNA substrate, potentially lowering the role of OGG1 in gene expression. To investigate the possible phosphorylation of OGG1 at S326, HEK293 cells were transfected with a Flag-tagged WT-OGG1-expressing plasmid. Immunoprecipitation (IP) assay revealed a high level of phosphorylation of OGG1 under normal condition. However, this phosphorylation rapidly decreased in response to TNFα stimulation, reaching its lowest level at 60 min. Notably, between 120 and 180 min, the phosphorylation level gradually restored (Fig. 7*A* and *SI Appendix*, Fig. S7*A*). The treatment with NAC attenuated the dephosphorylation of OGG1, indicating the implication of ROS in dephosphorylation of OGG1 (Fig. 7*B* and *SI Appendix*, Fig. S7*B*).

To identify the kinase responsible for OGG1 phosphorylation, the whole cell lysates of HEK293 cells were collected to analyze the OGG1-related interactome. Protein mass spectrometry analysis showed a coprecipitation of CDK4 with OGG1 (*SI Appendix*, Table S2). The direct interaction between OGG1 and CDK4 was also confirmed through co-IP and PLA (Fig. 7 *C–E* and *SI Appendix*, Fig. S7 *C* and *D*). After 1-h TNFα stimulation, the interaction between OGG1 and CDK4 decreased, but was restored at 3 h post TNFα stimulation. RelA/p65 was observed in the OGG1-precipitated complex, whereas PKCα was absent, in line with our previous study (24), Intriguingly, the interaction of OGG1 with CDK4 displayed a kinetics opposite to its interaction with RelA/p65 (*SI Appendix*, Fig. S7 *E* and *F*). These results suggested that OGG1 maintains a high level of constitutive phosphorylation under basal conditions, and undergoes dephosphorylation upon inflammatory stimulation, potentially benefiting its function in transcriptional activation.

A previous prediction suggested that Ser326 of OGG1 is likely a phosphorylation site (35). To test, both WT-OGG1 and OGG1S326C were overexpressed in HEK293 cells and IP experiments were performed. The results showed that WT-OGG1 exhibited a high level of serine phosphorylation under the basal condition, which was decreased at 60 min after stimulation with TNFα. In contrast, OGG1S326C displayed a lower level of serine phosphorylation under basal condition, which remained unchanged upon TNFα stimulation (Fig. 7*F* and *SI Appendix*, Fig. S7*G*), implying that S326 of OGG1 is one of the sites. The Group-based Prediction System (GPS) 5.0 (kinase-specific phosphorylation site prediction (biocuckoo.cn) revealed S231, S232, and S326 as potential phosphorylation sites, with S326 particularly relevant to the hOGG1S326C variant. To confirm this, LC–MS/MS was utilized to analyze the phosphorylated site(s) of OGG1. Using the Byonic engine, phosphorylated peptide FSADLRQPSRHAQEPPAKRRKGSKGPEG was identified [PXD059565] (36) (note the bold and underlined serine) (Fig. 7*G*).

To confirm the phosphorylation at site 326 of OGG1, a customized antibody (Ab) specific for detecting OGG1S326 phosphorylation was developed. A dot-blot assay validated the immunoreactivity and the specificity of this Ab (Fig. 7*H*). Subsequently, an in vitro kinase assay was conducted by using recombinant proteins to detect the phosphorylation of OGG1 at S326. The level of OGG1 phosphorylation was assessed using a pan-phosphoryl Ab as well as our customized Ab specific for phosphorylated S326 of OGG1. The results showed that S326 was one of the major sites of OGG1 undergoing phosphorylation (Fig. 7 *I* and *J*). Moreover, we established a compatible expression system by coexpressing His-CDK4 with GST-OGG1 in *Escherichia coli*.

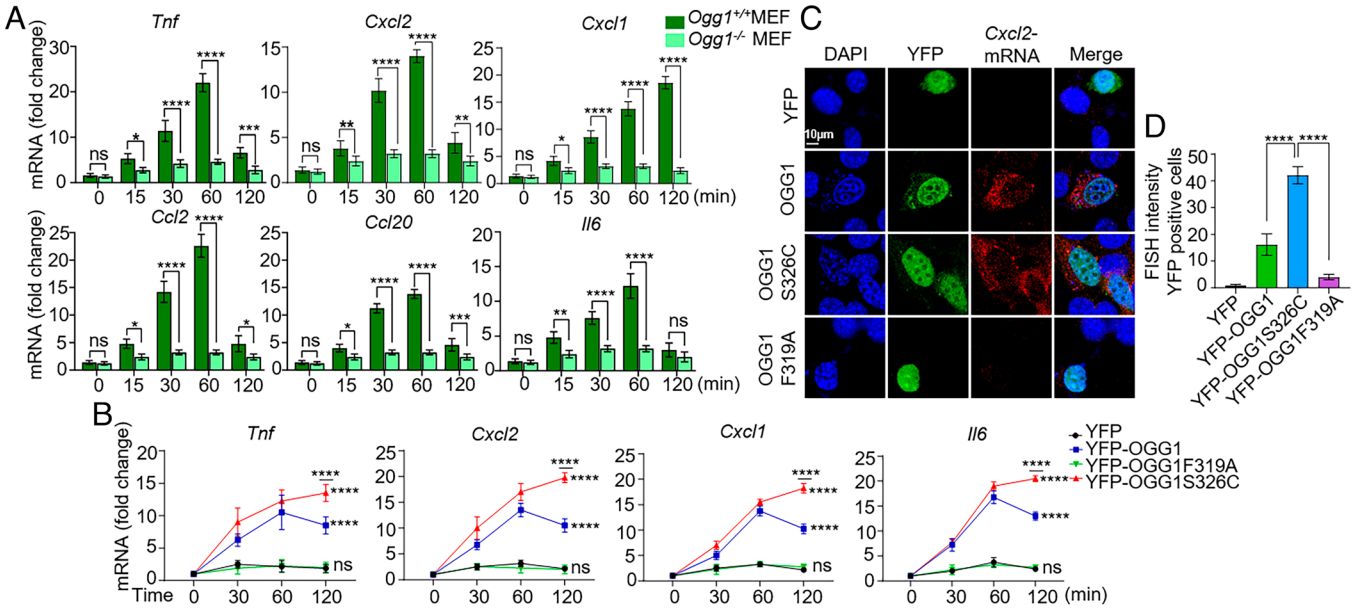


**Fig. 3.** OGG1S326C is more potent to activate transcription from proinflammatory genes than WT -OGG1. (*A*) The kinetics of inflammatory gene expression in response to TNFα stimulation in *Ogg1*$^{+/+}$ and *Ogg1*$^{-/-}$ MEF cells. Cells were stimulated with TNFα (20 ng/mL) for 0, 15, 30, 60, and 120 mins. RT-qPCR was conducted to analyze the expression at mRNA levels of selected inflammatory genes. (*B*) Sustained gene expression in OGG1S326C-expressing cells. *Ogg1*$^{-/-}$ MEF cells expressing YFP, YFP-OGG1, YFP-OGG1S326C, or YFP-OGG1F319A were exposed to TNFα (20 ng/mL) for increasing lengths of time as indicated. Expression of *Tnf-α*, *Cxcl2*, *Cxc1*, *Il6* was determined by RT-qPCR, with that in YFP-transfected cells serving as control. (*C* and *D*) Increased expression of *Cxcl2* mRNA in OGG1S326C-expressing *Ogg1*$^{-/-}$ MEF cells as determined by fluorescence in situ hybridization (FISH). Cells were exposed to TNFα (20 ng/mL) for 60 min and processed for FISH as described in *Materials and Methods*. The nuclei of cells were counterstained with DAPI (blue). *Cxcl2* mRNA (red); and OGG1 (green). (Scale bar, 10 μm.) (*C*). Quantification of gene expression in YFP-positive cells is shown in (*D*) (>50 cells were evaluated per sample). The data are presented as the means ± SEM. A one-way ANOVA was used to determine statistical significance in (*A*) and (*D*). A two-way ANOVA was used in (*B*). *$P$ < 0.05, **$P$ < 0.01, ***$P$ < 0.001, ****$P$ < 0.001, ns: not significant.

The phosphorylation of purified GST-tagged WT-OGG1 was detected using pan-phosphoryl and the customized anti-p-OGGS326 Abs. The results also showed that the S326 of OGG1 was one of major phosphorylation sites (Fig. 7*K*). Importantly, in HEK293 cells, the phosphorylation of S326 of OGG1 was decreased following CDK4 knockdown. TNFα stimulation induced significant dephosphorylation at S326 of OGG1, a phenomenon not observed in CDK4 knockdown cells (Fig. 7 *L* and *M* and *SI Appendix*, Fig. S7 *H–J*), suggesting CDK4-mediated phosphorylation of S326 and inflammation-triggered dephosphorylation may constitute a regulatory cycle.

**Dephosphorylation at S326 Facilitates OGG1 Binding with DNA Substrate and Promotes Gene Expression.** We proposed that phosphorylation/dephosphorylation of S326 constitutes a regulatory

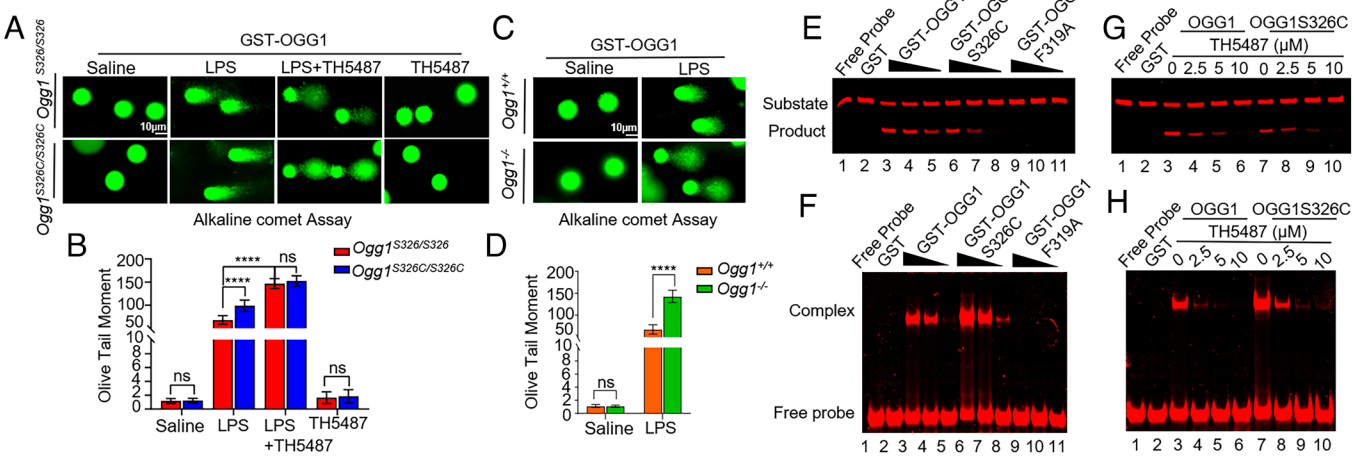


**Fig. 4.** Increased accumulation of genomic 8-oxoGua in lungs of OGG1S326C-expressing mice as shown by FLARE comet assays. (*A-D*) FLARE comet images of cells from the lungs of the mice homozygous for *Ogg1*$^{S326C/S326C}$ and *Ogg1*$^{S326/S326}$, or *Ogg1*$^{+/+}$ and *Ogg1*$^{-/-}$, with or without LPS challenge. Lungs from mice were collected, and FLARE comet assays performed (*Materials and Methods*). Shown are the representative Olive Tail Moments (OTM) images of the genome (*A* and *C*), and the corresponding OTM values are shown in (*B* and *D*). (Scale bar, 10 μm.) In (*B*) and (*D*), statistics were derived from at least 80 cells. Data are expressed as mean ± SEM. Significance was determined by using one-way ANOVA. *$P$ < 0.05, **$P$ < 0.01, ***$P$ < 0.001, ****$P$ < 0.001, ns: not significant. (*E*) OGG1S326C exhibits lower base excision ability than wt-OGG1. Cleavage assays were performed as described in the Material and Method section to compare the excision of substrate by WT -OGG1 and OGG1S326C. OGG1F319A was used as a control. (*F*) Binding of OGG1S326C with the DNA substrate is higher than that of WT -OGG1. EMSAs were conducted (Material and Method) to determine the levels of WT -OGG1 and OGG1S326C bound to substrate. OGG1F319A was used as a control. (*G* and *H*) The OGG1 inhibitor TH5487 prevents both substrate binding and excision by OGG1 and OGG1S326C. Cleavage assays and EMSA were performed (*Materials and Methods*) to evaluate the inhibition of 8-oxoGua excision by and binding of WT -OGG1 and OGG1S326C in the presence or absence of TH5487. In *E* and *F*, the concentrations of GST-fused proteins were 20, 10, or 5 nM. In *G* and *H*, the concentrations of GST or GST-fused proteins were 10 nM.

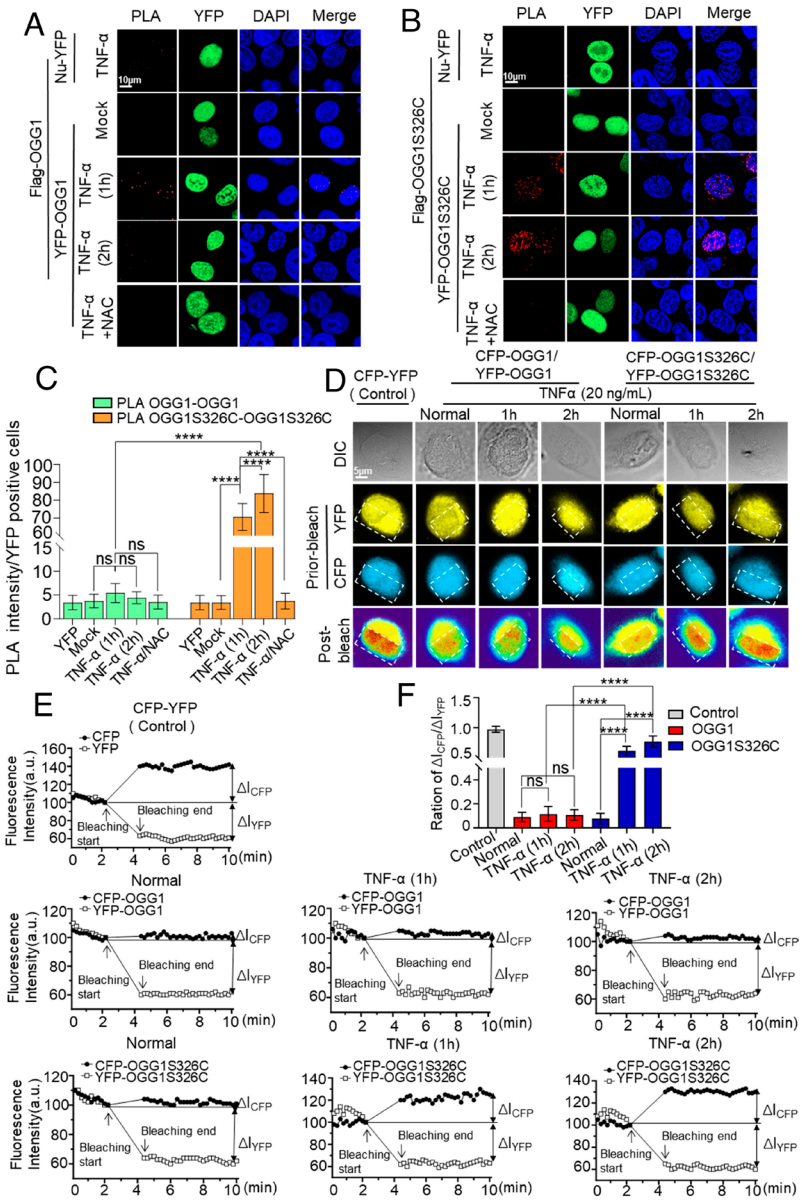


**Fig. 5.** Inflammatory cytokine TNFα exposure of cells increases levels of OGG1S326C dimerization. (*A* and *B*) Intermolecular interaction between OGG1S326C molecules is associated with the nonsoluble chromatin fraction. HeLa cells were cotransfected with plasmids expressing YFP-OGG1 and Flag-OGG1 (*A*) or YFP-OGG1S326C and Flag-OGG1S326C (*B*). Cells were exposed to TNFα (20 ng/mL) for 60 and 120 min, with or without prior treatment with NAC (5 mM). Thereafter, cells were processed in CSK buffer and fixed with 4% paraformaldehyde for 10 min. PLA was performed as in *Materials and Methods*. (Scale bar, 10 μM.) (*C*) Graphical depiction of dimerization of OGG1 variants. The number of red foci in the nuclei of >8 cells per experimental group was quantified using Image-J. The data are presented as the means ± SEM, and significance was assessed using one-way ANOVA. $*P < 0.05$, $**P < 0.01$, $***P < 0.001$, $****P < 0.001$, ns: not significant. (*D*) Interactions between OGG1S326C molecules shown by FRET analysis. HeLa cells coexpressing CFP and YFP-tagged WT -OGG1 or CFP and YFP-tagged OGG1S326C were treated with TNFα (20 ng/ mL) for 60 and 120 min or not. FRET analysis was performed post YFP photobleaching (*Materials and Methods*). Cells expressing CFP-YFP fused protein were taken as the positive control. (Scale bar, 5 μM.) (*E*) Graphical illustration of FRET as a function of time. HeLa cells as described in panel to D were treated with TNFα (20 ng/ mL) and subjected to FRET analysis. Cells expressing fused CFP-YFP were taken as the positive control. Quantitative analysis of the $\Delta I_{CFP}/\Delta I_{YFP}$ ratio was performed as described in *Materials and Methods*. $\Delta I_{CFP}$ is the increase of CFP intensity, and $\Delta I_{YFP}$ represents the decrease of YFP intensity. Initial intensities were normalized to 100. Data were obtained from 15 to 20 cells in three independent experiments. (*F*) Quantitative analysis of the $\Delta I_{CFP}/\Delta I_{YFP}$ ratio. Analysis was performed as described in *Materials and Methods*. The data are presented as the means ± SEM. Statistical significance was determined using one-way ANOVA. $*P < 0.05$, $**P < 0.01$, $***P < 0.001$, $****P < 0.001$, ns: not significant. Abbreviations: FRET, Fluorescence Resonance Energy Transfer; CFP, Cyan Fluorescent Protein; YFP, Yellow Fluorescent Protein.

mechanism for OGG1's role in transcriptional regulation. To test this hypothesis, recombinant proteins including GST-OGG1, GST-OGG1S326C, GST-OGG1S326E (mimicking phosphorylated S326 of OGG1) were purified. The effects of phosphorylation on the binding and cleavage abilities of OGG1 and its variants were assessed using cleavage assay and EMSA experiments (*SI Appendix*, Fig. S4 *A–D*). The results revealed that the cleavage activity of OGG1S326E was comparable to that of wt-OGG1, but its ability to bind DNA substrate was markedly lower (Fig. 8 *A* and *B* and *SI Appendix*, Fig. S8 *A* and *B*).These seemingly contradictory results may be explained as that the phosphorylation of S326 does not impair OGG1 in recognition and excision of its substrate; however, the introduction of negative charge at position S326 of OGG1 may affect the affinity of OGG1 for DNA, leading to a decreased binding of OGG1 with DNA and resulting in a separation of protein with the DNA probe under electrophoresis condition.

Moreover, WT-OGG1 and OGG1S326E expression plasmids were transfected into *Ogg1*$^{-/-}$ MEF cells, followed by inflammatory stimulation with TNFα for 60 min. RT-qPCR analysis showed that cells expressing OGG1S326E exhibited lower expression of *Tnf-α*, *Cxcl1*, *Il6,* and *Cxcl2* compared with cells expressing WT-OGG1 (Fig. 8*C* and *SI Appendix*, Fig. S9*A*). ChIP assay revealed that the association of OGG1S326E with promoter regions of these proinflammatory genes was decreased, which corresponds to lower NF-κB occupancy at promoters (Fig. 8 *D* and *E*). The result of PLA showed that wt-OGG1 had significantly higher ability to interact with NF-κB than OGG1S326E in response to TNFα exposure. (Fig. 8 *F–H*). Subsequently, siRNA targeting CDK4 resulted in a decreased phosphorylation level of OGG1 in HEK293 cells (Fig. 9*A* and *SI Appendix*, Fig. S9 *B* and *C*); and correspondingly, the expression of *CXCL2*, *IL6*, and *TNF-α* increased compared with the control group. Moreover, upon TNFα stimulation, the expression of these genes was significantly higher in the si-CDK4-transfected group compared with that in the control siRNA-transfected group (Fig. 9*B*).

To further validate the significance of eliminating S326 phosphorylation under inflammatory conditions, plasmids expressing GFP-tagged mouse *Ogg1*, as well as GFP-*Ogg1*S326(H) and GFP-*Ogg1*S326C(H) mutants that resemble WT-hOGG1 and the hOGG1S326 variant, were constructed. The 326~330 amino acid PSLSR corresponding mouse *Ogg1* gene was mutated into human-derived SRHAQ and CRHAQ respectively, yielding the constructs namely GFP-*Ogg1*S326(H) and GFP-*Ogg1*S326C(H) (Fig. *9C*). These plasmids were then transfected into HEK293 cells. The phosphorylation levels of OGG1 and its variants were examined by using the Ab against phosphoryl-S326 of OGG1. GFP-*Ogg1* exhibited a considerable level of phosphorylation, implying a potential phosphorylation at S327 or S329 of wt-mouse Ogg1, which may be recognized by the Ab against phosphoryl-S326 of

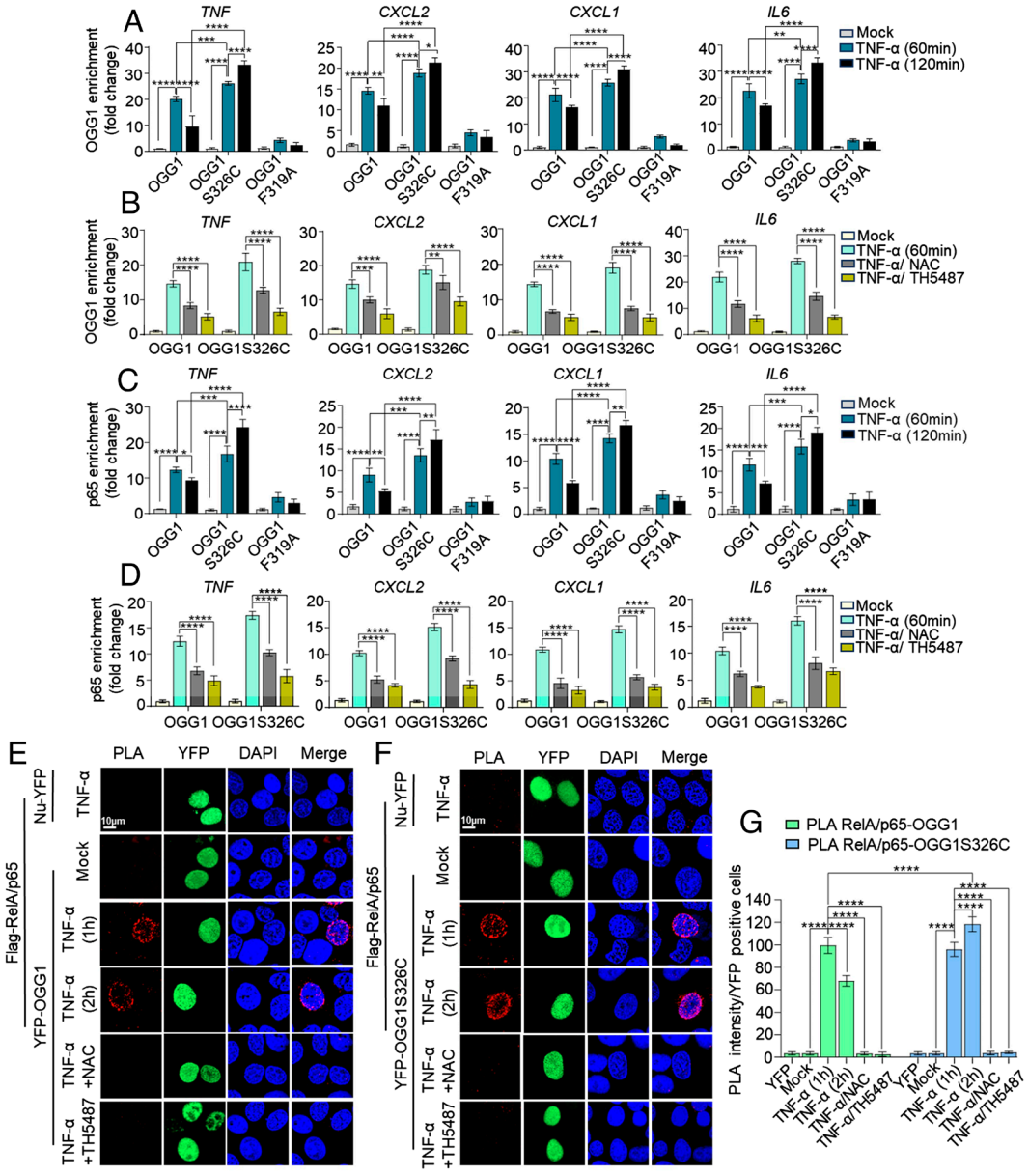


**Fig. 6.** Increased proinflammatory cytokine and chemokine expression is associated with enhanced levels of OGG1S326C bound to promoter sequences. (*A*) Enhanced recruitment of OGG1S326C to the promoter regions of inflammatory genes compared with that of WT-OGG1. Parallel cultures of HEK293 cells expressing Flag-OGG1, Flag-OGG1S326C, or Flag-OGG1F319A were exposed to TNFα (20 ng/mL) for 60 and 120 min. ChIP assays were performed using OGG1 antibody followed by qPCR. (*B*) Association of OGG1 and the variants with promoter sequences are oxidative stress dependent. HEK293 cells expressing Flag-OGG1 and Flag-OGG1S326C were either mock-treated or pretreated with NAC (5 mM) or TH5487 (10 μM) for 30 min, and then exposed to TNFα (20 ng/mL) for 60 min. ChIP assays were performed as described above. (*C*) Increased DNA occupancy of NF-κB in OGG1S326C-expressing cells, compared to that in cells expressing WT-OGG1. HEK293 cells expressing Flag-OGG1, Flag-OGG1S326C, or Flag-OGG1F319A were exposed to TNFα (20 ng/mL) for 60 and 120 min. ChIP assays were performed using RelA/p65 antibody followed by qPCR. (*D*) Oxidative stress-dependent increases in NF-κB levels at promoters in OGG1S326C-expressing cells. HEK293 cells expressing Flag-OGG1 or Flag-OGG1S326C were mock or pretreated with NAC (5 mM), or TH5487 (10 μM), and subsequently exposed to TNFα (20 ng/mL) for 60 min. All ChIP experiments were performed three times with data expressed as mean ± SEM. Statistical significance was determined by one-way ANOVA. $*P < 0.05$, $**P < 0.01$, $***P < 0.001$, $****P < 0.001$, ns: not significant. (*E-G*) Induction of interaction between OGG1S326C and NF-κB is higher compared with that of WT-OGG1, as shown by PLA. Parallel cultures of HeLa cells coexpressing YFP-OGG1 and Flag-RelA/p65 (*E*), or YFP-OGG1S326C and Flag-RelA/p65 (*F*), were treated with TNFa (20 ng/mL), TNFa +NAC (5 mM), or TNFa+TH5487 (10 μM). PLAs were performed as in *Materials and Methods*. Shown are representative images of different groups. (Scale bar, 10 μM.) The quantification was shown in (*G*). Image-J was used to count the number of the red foci. Measurements were obtained from 8 to 10 cells in three independent experiments. Data are expressed as mean ± SEM. One-way ANOVA was used to analyze significance of differences. $*P < 0.05$, $**P < 0.01$, $***P < 0.001$, $****P < 0.001$, ns: not significant.

OGG1. GFP-Ogg1S326(H) showed a markedly higher level of phosphorylation. In response to TNFα, the phosphorylation of both GFP-Ogg1 and GFP-Ogg1S326(H) was decreased. However, no phosphorylation was detectable by Ab against phosphoryl-S326 of OGG1 in the GFP-Ogg1S326C(H)-expressing group (Fig. 9*D* and *SI Appendix*, Fig. S9*D*). These plasmids were then transfected into *Ogg1*$^{-/-}$ MEF cells. One-hour TNFα exposure induced a similar increase in the expression of proinflammatory cytokines and chemokine in cells transfected with GFP-Ogg1 and GFP-Ogg1S326(H). However, compared with that in these two groups, the upregulation of gene expression in the cells transfected with GFP-Ogg1S326C(H) was significantly higher (Fig. 9*E*).

Finally, C57BL/6JGpt mice, *Ogg1*$^{S326/S326}$ mice, and *Ogg1*$^{S236C/S326C}$ mice were subjected to intranasal administration of LPS (10 mg/kg) for 2 h, and the phosphorylation levels of OGG1 were detected using the customized Ab specific against OGG1 phospho-S326. Both C57BL/6JGpt and *Ogg1*$^{S326/S326}$ exhibited a markedly higher level of Ogg1 phosphorylation, upon LPS stimulation, which significantly decreased in lungs of *Ogg1*$^{S326/S326}$ mice. This phosphorylation was also moderately decreased in lungs of C57BL/6JGpt, suggesting S327 or S329 of murine Ogg1 may undergo phosphorylation and subsequent dephosphorylation. Notably, no Ogg1 phosphorylation was detectable in lungs of *Ogg1*$^{S236C/S326C}$ mice with or without LPS stimulation (Fig. 9 *F* and *G*). Taken together, these data suggest that S326 of hOGG1 is an important site for serine phosphorylation, and the dephosphorylation of hOGG1 enhances its function in gene transcription activation. The replacement of serine with cysteine at site 326 not only exempts the phosphorylation-introduced impairment, but also enhances the function of OGG1 in transcription activation (Fig. 10).

## Discussion

8-OxoGua is one of the most prevalent forms of oxidative DNA base damage, and OGG1 is traditionally recognized as a cognate DNA repair enzyme that initiates BER pathway to maintain genome fidelity (37). Given the potential mutagenicity associated with 8-oxoGua, the etiologic link between the allelic *OGG1*$^{S326C}$ and disease susceptibility

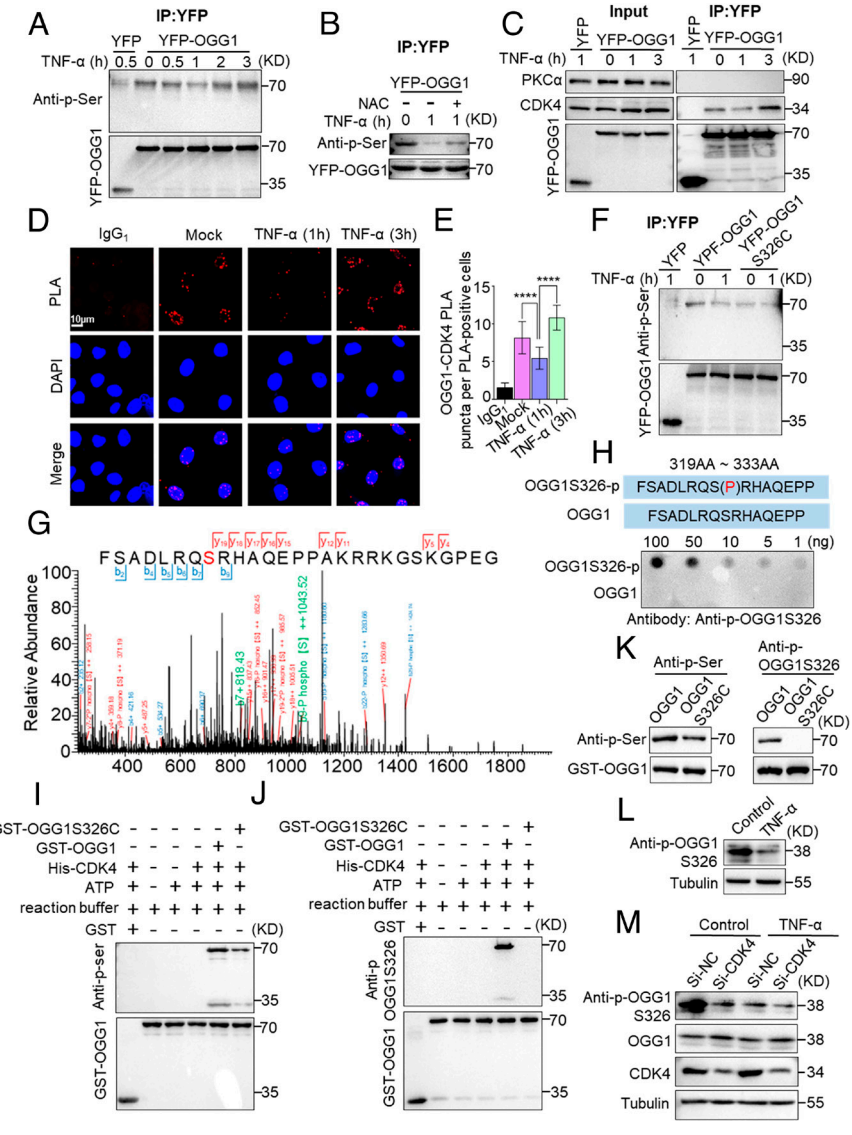


**Fig. 7.** Inflammatory stimulation leads to dephosphorylation of OGG1 at S326. (*A*) Changes in phosphorylation level of WT-OGG1 upon inflammatory stimulation. HEK293 cells expressing YFP-OGG1 ± NAC (5 mM) were exposed to TNFα (20 ng/mL) for 0, 15, 30, 60, 120, and 180 min, and then IP assays were performed using YFP antibody (Ab). The phosphorylation level of OGG1 was detected by serine Pan-phosphoryl Ab. (*B*) Oxidative stress induces OGG1 undergoing dephosphorylation. HEK293 cells were mock-treated or exposed to TNFα (20 ng/mL) for 1 h with or without NAC pretreatment. The phosphorylation level of OGG1 was detected by serine Pan-phosphoryl Ab. (*C*) OGG1 interacts with CDK4 but not PKCα in TNFα-exposed cells. HEK293 cells expressing YFP or YFP-OGG1 were exposed to TNFα (20 ng/mL) for 0, 60, and 180 min, and then IP assays were performed by using YFP Ab. Western blot analysis shows the interactions of OGG1 with indicated kinases. (*D* and *E*) Kinetics interactions between OGG1 and CDK4 in nuclei of cells exposed to TNFα. HeLa cells were exposed to TNFα (20 ng/mL) for 0, 60, and 180 min, and PLAs were performed by using $IgG_1$ or Ab to OGG1 and CDK4. Red foci in the nucleus show the interaction between OGG1 and CDK4. (Scale bar, 10 μM.) (*D*). Images represent three independent experiments in triplicate. Image-J was used to quantify the number of red foci in nuclei across groups (*E*). *t* test analysis was performed to evaluate the significance of differences: ****$P < 0.001$. (*F*) OGG1S326C shows a lower serine phosphorylation level compared with its WT counterpart. HEK293 cells expressing YFP-OGG1 or YFP-OGG1S326C were exposed to TNFα (20 ng/mL) for 60 min, followed by IP using YFP Ab. The phosphorylation of OGG1 was detected with a Pan-phosphoryl Ab via western blotting. (*G*) S326 is the major site of OGG1 undergoing phosphorylation. An in vitro kinase reaction was set up by incubating recombinant proteins His-CDK4 and GST-OGG1 in the presence of ATP, and then phosphorylation of OGG1 was analyzed by LC–MS/MS. Data were processed with the Byonic engine. The peptide containing phosphorylated S326 was identified with the y and b fragmentations mapping the phosphorylation site to the Ser (indicated in red). (*H*) Characterization of the customized antibody against phosphor-OGG1S326. Decreasing concentrations of phosphorylated OGG1S326 (OGG1-S326-p) and unphosphorylated OGG1S326 peptides were spotted on nitrocellulose membrane, and then probed with the customized anti-p-OGG1S326 Ab to confirm the immunoreactivity and specificity. (*I*-*K*) CDK4 is responsible for OGG1S326 phosphorylation. In vitro kinase assays were performed using recombinant His-CDK4, GST-OGG1, and the GST-OGG1S326C variant in the presence of ATP. OGG1 phosphorylation was detected via western blot using pan-phosphoryl (*I*) and customized anti-p-OGGS326 Abs (*J*). A compatible expression system was established by coexpressing His-CDK4 with GST-OGG1 in *Escherichia coli*, the phosphorylation of purified GST-tagged WT OGG1 was detected with pan-phosphoryl and the customized anti-p-OGGS326 Abs (*K*). (*L*) Phosphorylation of WT-OGG1 declines upon TNFα exposure. HEK293 cells were stimulated with TNFα (20 ng/mL) for 1 h, and then lysed. Phosphorylation of OGG1 was detected by using customized anti-p-OGGS326 antibody. (*M*) Depletion of CDK4 by siRNA decreases the phosphorylation of WT-OGG1. HEK293 cells with or without prior CDK4 knock-down were exposed to TNFα (20 ng/mL) or not for 1 h, and whole cell lysates were collected followed by analysis of OGG1 phosphorylation using the customized anti-p-OGG1S326 Ab. Abbreviations: CDK4, Cyclin-dependent kinase-4; PKCα, Protein Kinase C alpha; IP, immunoprecipitation.

is often attributed to the decreased repair activity of this OGG1 variant (29, 31, 38–40). Recently, it has been acknowledged that promoter-bound OGG1 functions as a key node, coupling DNA damage repair to the transcriptional activation of proinflammatory genes by recruiting transcription factors (4, 22). The present study extends this new concept, linking the role of OGG1S326C variant in transcription regulation to the susceptibility of the individuals carrying the allelic *OGG1*$^{S326C}$ genotype to inflammation-related diseases. Compared with WT-OGG1, OGG1S326C displays a prolonged association with DNA substrates despite its impaired enzymatic activity. Consequently, it induces not only elevated but also sustained expression of proinflammatory cytokine and chemokine genes in response to inflammatory challenges. In contrast, WT-hOGG1, the counterpart of this variant, typically exists in a highly phosphorylated state due to CDK4-mediated phosphorylation at S326. This phosphorylation decreases OGG1's affinity for DNA substrates. Upon inflammatory stimulation, WT-hOGG1 undergoes dephosphorylation, restoring its DNA binding capability and facilitating the expression of proinflammatory cytokines and chemokines.

The functional characterization of OGG1S326C has long been inconclusive. OGG1S326C has been reported to be either less efficient in base excision than WT-OGG1 or to exhibit equivalent in *E. coli* mutator strain complementation tests (6, 17). Additionally, cell extracts of lymphocytes from individuals carrying homozygous of *hOGG1*$^{S326}$ or *hOGG1*$^{S326C}$ also yielded seemingly contradictory results. For instance, one study reported that OGG1 with the S326 polymorphism had an activity of 33.0 ± 4.9 fmol, while that with Cys326 polymorphism was 33.2 ± 7.1 fmol, showing no significant difference in OGG1 activity to excise 8-oxoGua (P = 0.8) (7). Conversely, another study found that cells with Cys/Cys genotype showed lower OGG1 activity and higher genetic instability especially under oxidative stress conditions (38). Importantly, treatment with the reducing agent (DTT) restored the 8-oxoGua excision ability of cells expressing the Cys variant to levels equivalent to those of wt-OGG1 (29). This study also highlights the critical impact of the oxidation state of Cys326 site on the function of OGG1, suggesting that individuals homozygous for the OGG1-Cys variant are more prone to accumulation of mutations under conditions of oxidative stress (28). Indeed, studies have reported

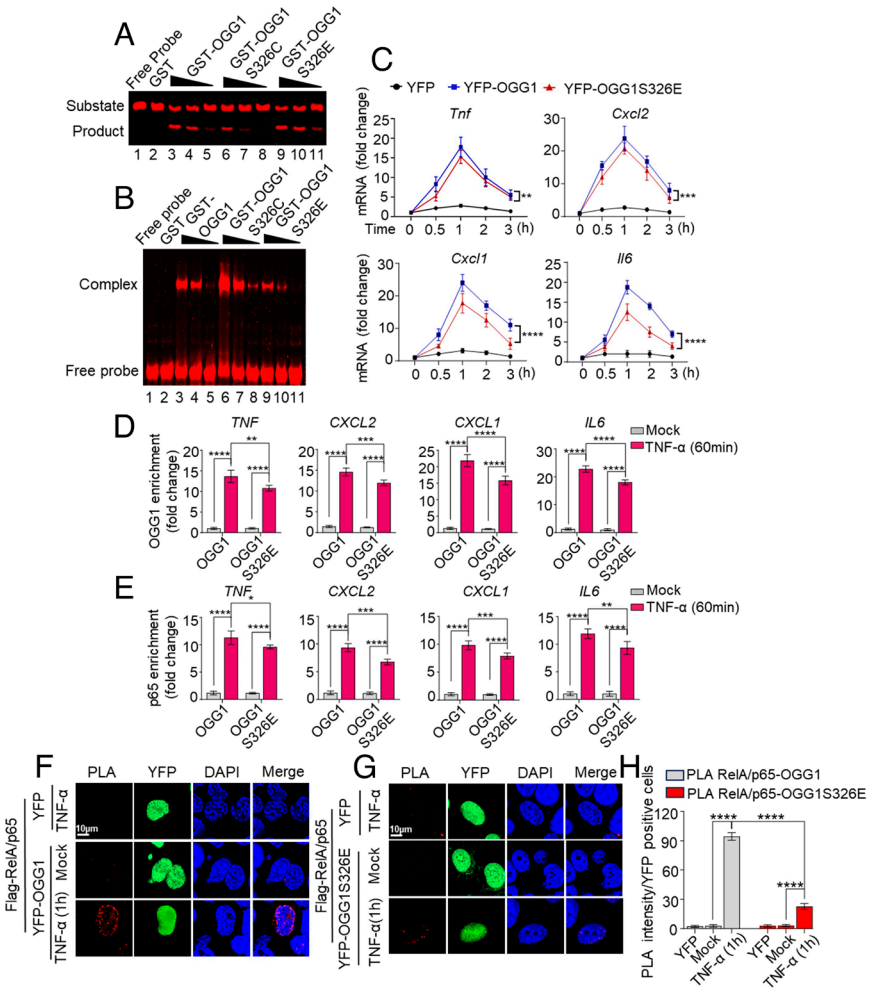


**Fig. 8.** Dephosphorylation of OGG1 at S326 facilitates its binding to DNA and the recruitment of NF-κB. (*A* and *B*) Binding to and DNA substrate excision by OGG1 variants. Cleavage and EMSAs were performed as in *Materials and Methods*. The concentrations of GST-fused proteins were 20, 10, or 5 nM, and that of GST was 10 nM. (*C*) Substitution of Serine 326 with Glutamine decreases the ability of OGG1 in upregulating the expression of proinflammatory genes. *Ogg1*$^{-/-}$ MEF cells were transfected with plasmids expressing YFP, YFP-OGG1, or YFP-OGG1S326E. Cells were then exposed to TNFα (20 ng/mL) for increasing length of time. Expression of *Tnf-α*, *Cxcl2*, *Cxcl1*, *Il6* was determined by RT-qPCR. The levels of gene expression in cells expressing YFP alone were used as controls. (*D* and *E*) Phosphorylation of OGG1 affects the recruitment of NF-κB to proinflammatory gene promoters during inflammatory stimulation. HEK293 cells expressing Flag-OGG1 or Flag-OGG1S326E were exposed to TNFα (20 ng/mL) for 60 min. ChIP assay was performed using an OGG1 (*D*) or a RelA/p65 antibody (*E*) followed by qPCR. (*F-H*) Interaction of wt-OGG1 with RelA/p65 upon TNFa exposure is more intensive than that of OGG1S326E. HeLa cells coexpressing YFP-OGG1 and Flag-RelA/p65 (*F*), or YFP-OGG1S326E and Flag-RelA/p65 (G), were treated with TNFα (20 ng/mL), and PLA was performed using YFP and Flag antibodies. Red foci in the nuclei show the interactions. (Scale bar, 10 μM.) Images represent three independent experiments performed in triplicates. The quantification was shown in (*H*). Image-J was used to count the number of the red foci. Measurements were obtained from 8 to 10 cells in three independent experiments. In *C*, *D*, *E*, and *H*, the data are presented as the means ± SEM. One-way ANOVA was used to determine statistical significance in *D*, *E*, and *H*, and two-way ANOVA was used in *C* to analyze significance of differences. **P* < 0.05, ***P* < 0.01, ****P* < 0.001, *****P* < 0.001, ns: not significant.

that OGG1S326C undergoes oxidation and dimerization, which leads to the impairment of OGG1 activity (29, 41, 42).

The cysteine residues of OGG1 particularly at position 326 are oxidized under oxidative stress. This oxidative stress promotes the formation of intermolecular disulfide bonds and leading to dimerization and decreased substrate excision from DNA (29, 42), which significantly reduces repair efficiency. In the present study, under physiological conditions (without inflammatory challenge), mice with the *Ogg1*$^{S326C/S326C}$ genotype did not accumulate 8-oxoGua similar to WT *Ogg1*$^{S326/S326}$ mice. These observations from *Ogg1*$^{S326C/S326C}$ mice mirror findings in cells derived from individuals carrying *OGG1*$^{S326C}$ allele, where background levels of 8-oxoGua were similar to those expressing WT-hOGG1 (6, 7). These findings suggest that OGG1S326C may repair 8-oxoGua comparable to WT-OGG1 under physiological levels of ROS, albeit with relative delayed process. In inflammatory conditions, which are known to increased ROS levels, the accumulation of 8-oxoGua in DNA elevates, implying a decrease in the cleavage activity of OGG1S326C, likely due to dimerization and/or a lack of APE1-mediated enhancement of OGG1 turnover on its substrate. While this decrease in repair activity was observed during a short experimental period, we suggest shifting attention to the prolonged and enhanced binding of OGG1S326C to 8-oxoGua. This characteristic signifies its potential role in transcriptional regulation.

When we compare the functions of OGG1S326C with its wt counterpart, the potential phosphorylation of the serine residue at site 326 of OGG1 becomes critically important. An earlier study utilized the NetPhos 2.0 server (https://services.healthtech.dtu.dk/services/NetPhos-3.1/), a neural network that predicts the probability of phosphorylation at specific site, and revealed that S326 had the highest score (>0.99) among all sites (43). In the present study, we employed the GPS 5.0 online tool for kinase-specific phosphorylation site prediction (biocuckoo.cn), and confirmed that S326 is one of the potential phosphorylation sites of OGG1. In support, a previous study revealed that the phosphor-mimetic substitution of Ser to Glu at position 326 (S326E) in OGG1 resulted in the decrease in release of 8-oxoGua from DNA. Moreover, while APE1 enhances the turnover rate of WT-OGG1 on its DNA substrate, it did not affect that of the OGG1S326E phosphor-mimetic mutant (41). In the present study, we showed that, compared with WT-OGG1, OGG1S326E possesses a significantly lower DNA binding ability although it has comparable cleavage activity. This finding not only explains why APE1 could not enhance the turnover rate of OGG1S326E phosphor-mimetic mutant, but also suggests that phosphorylation of hOGG1 at S326 may be unfavorable for its role in transcription regulation. Moreover, while early studies showed that the serine/threonine residues in OGG1 could be phosphorylated by CDK4 or PKC in vitro (32, 33), we utilized LC–MS/MS and the Byonic engine in our current study to precisely identify S326 as the phosphorylation site targeted by CDK4. Importantly, utilizing a customized anti-p-S326 Ab, we confirmed that CDK4 phosphorylates OGG1 at S326 in vivo. Under physiological conditions, OGG1 exhibits high level of this phosphorylation. However, upon inflammatory stimulation, dephosphorylation of OGG1 at S326 occurs, serving as a regulatory mechanism that modulates OGG1's involvement in gene transcription regulation.

In the present study, we observed a high basal level of OGG1 phosphorylation at S326 mediated by CDK4. This modification decreases upon inflammatory stimulation, allowing OGG1 to acquire higher DNA binding affinity to fulfill the requirement for its function in gene transcription regulation. These findings raise a key question: what is the significance of OGG1 bearing such a high level of constitutive phosphorylation at S326? Given that the CDK4/6 complex governs G1

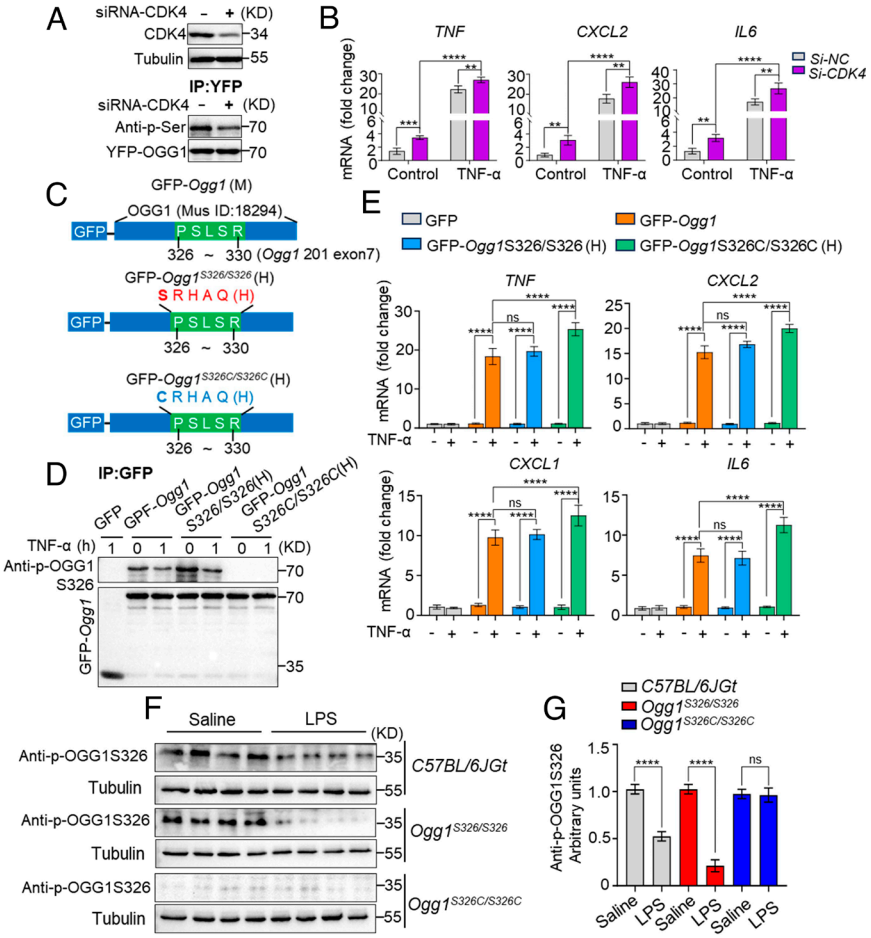


**Fig. 9.** Decrease in CDK4-mediated phosphorylation of OGG1 at S326 enhances proinflammatory gene expression. (*A* and *B*) CDK4 knockdown increases proinflammatory gene expression. The efficacy of CDK4 knockdown was performed and confirmed as in *Materials and Methods*. OGG1 phosphorylation levels was assessed using pan-phosphoryl antibody (Ab) (*A*). HEK293 cells were exposed to TNFα (20 ng/mL) for 60 min. Expression of *TNF-α*, *CXCL2*, *IL6* was determined by RT-qPCR. The levels of gene expression in cells transfected with control siRNA with no TNFα exposure were used as controls (*B*). (*C-E*) Decrease in phosphorylation of OGG1 at S326 promotes proinflammatory gene expression. A schematic diagram illustrates plasmids expressing GFP-tagged mouse Ogg1, along with mouse Ogg1-based human WT-OGG1 and OGG1S326C, namely GFP-Ogg1S326(H) and GFP-Ogg1S326C(H) (*C*). *Ogg1*$^{-/-}$ MEF cells expressing GFP-Ogg1, GFP-Ogg1S326(H), or GFP-Ogg1S326C(H) were exposed to TNFα (20 ng/mL) for 60 min. Western blotting was performed to detect OGG1 phosphorylation using anti-phosphoryl-S326 Ab (*D*). Expression of *TNF-α*, *CXCL2*, *CXCL1*, *IL6* was determined by RT-qPCR. Cells expressing GFP-Ogg1 with no TNFα exposure served as control (*E*). (*F* and *G*) Decrease in phosphorylation upon LPS challenge of lungs in *Ogg1*$^{S326C/S326C}$ mice. C57BL/6JGpt mice and *Ogg1*$^{S326/S326}$ and *Ogg1*$^{S326C/S326C}$ mice were subjected to intranasal administration of LPS (10 mg/kg, for 2 h), with mice administrated physiological saline serving as control. Phosphorylation of OGG1 at site 326 was detected via western blot using anti-p-OGG1S326 Ab (control group n = 4, experimental group n = 4) (*F*). Quantitative analysis of OGG1 phosphorylation was performed using Image-J software (*G*). All experiments were performed three times. The data are presented as the means ± SEM. A one-way ANOVA was used to analyze the significance of differences. **P* < 0.05, ***P* < 0.01, ****P* < 0.001, *****P* < 0.001, ns: not significant.

phase of cell cycle, and our present study showed that OGG1S326E has lower DNA-binding activity, it is reasonable to propose that CDK4-mediated phosphorylation of S326 in OGG1 enhances its efficiency in searching DNA damage. The molecular dynamics by which OGG1 slides along DNA to locate and bind with the substrate has been of extensive scientific interest (44–50). For efficient target detection, OGG1 operates in at least two distinct DNA interacting modes: a low-affinity and nonspecific one that ensures a fast sliding along the DNA and searching out the rare 8-oxoGua lesion; and a tighter and more specific mode is associated with target recognition and binding. Obviously, other nuclear proteins contribute to enhancing these specific interactions of OGG1 (44–50). Since S326 is distant from the "active pocket" of OGG1, phosphorylation at this site introduces the negative charge to the disordered and basic amino acid-rich C terminal segment. This may neutralize the positive charges, promoting efficient genome searching without impairing the recognition and specific binding of the damaged site. Upon inflammatory stimulation, the decrease in S326 phosphorylation ensures a tighter binding of OGG1 to promoter-embedded substrates, accommodating transcription factors for prompt transcriptional activation of pro-inflammatory cytokines and chemokines. In this context, OGG1S326C, which intrinsically exhibits a higher affinity for substrates, may outperform dephosphorylated WT-OGG1 in upregulating gene transcription under oxidative stress conditions.

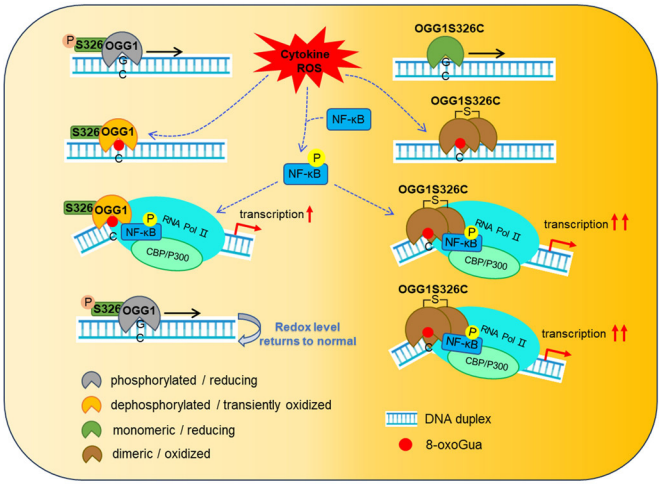


**Fig. 10.** Proposed model of gene expression by wt-OGG1 and the variant OGG1S326C. *Left* panel, dephosphorylation of OGG1 at S326 and its reversible oxidation facilitates its role in transcriptional activation. *Right* panel, sustained promoter occupancy of dimerized OGG1S326C promotes gene expression, leading to excessive expression of pro-inflammatory mediator and inflammation.

A previous study documented that OGG1S326C is more prone to dimerization compared to WT-OGG1, possibly through the Cys residue at position 326 (16). This early study suggested that physiologically relevant levels of TNF-α simultaneously induce 8-oxoGua formation and inactivate OGG1S326C, potentially contributing to an increased risk of cancer in *OGG1*$^{S326C}$ homozygous individuals. However, our present study offers a perspective on the impaired catalytic activity of OGG1 S326C. This decrease in 8-oxoGua repair efficiency leads to an enhanced and prolonged association with its DNA substrate, thereby is more effective to recruit transcription factors and induce the expression of pro-inflammatory cytokines and chemokines. Given the close association between inflammation and cancer, we propose that the pro-inflammatory propensity of OGG1S326C adds another layer of the cancer susceptibility in *OGG1*$^{S326C}$ homozygous individuals. A high frequency of *OGG1*$^{S326C}$ correlates with the prevalence of various lung cancers and other lung diseases that consistently rank among the most common illnesses in

Asia including China. These diseases are etiologically linked chronic inflammation caused by environmental exposures (51). Additionally, the inflammatory tumor microenvironment, characterized by excessive expression cytokines and chemokines, growth factors, as well as the enrichment of tumor-associated macrophages, and myeloid-derived suppressor cells, collectively promoting tumor progression and metastatic and invasion abilities (52–55).

Surprisingly, a study using a mouse model of inflammatory bowel diseases (IBD) found that $Ogg1^{-/-}$ mice exhibit milder symptoms compared with $Ogg1^{+/+}$ mice, as determined by colon histopathology (56). After dextran sulfate sodium salt challenge, the histopathology of wt-mice showed moderate ulcerative colitis, whereas $Ogg1^{-/-}$ mice displayed a severe ulcerative colitis phenotype along with alteration of microbiome and enrichment of pathogenic bacteria. In another study, $Ogg1^{-/-}$ mice fed a high-fat diet were more likely to be obese than $Ogg1^{+/+}$ mice (57). Epidemiological surveys indicate that the incidence of IBD and obesity is particularly high in western populations (58, 59). Considering that the frequency of $OGG1^{S326C}$ is 40 to 60 percent in Asian population, we speculate that $OGG1^{S326C}$ might constitute a protective factor in IBD and obesity. However, the underlying mechanisms remain to be elucidated and warrant further exploration. The fact that $OGG1^{S326C}$ has been preserved through natural selection among many SNPs of OGG1 and is among the most frequent variants suggest that this genotype is likely either beneficial or harmful depending on the disease contexts and types of implicated cells. In such contexts, distinct gene expression profiles influenced by OGG1 may play a pivotal role.

In summary, the present study provides data elucidating the etiological links between $OGG1^{S326C}$ and the susceptibility to inflammatory diseases. Mechanistically, the enhanced and prolonged engagement of OGG1S326C with its substrate, due to its compromised repair activity, renders it as a potential contributor to the induction of proinflammatory cytokines and chemokines. Based on these findings, using small molecules, like TH5487 and SU0268 (26, 60), to block the substrate binding site of both WT-OGG1 and OGG1S326C holds clinical potential for preventing or mitigating acute/chronic inflammatory responses.

## Materials and Methods

***Antibodies.*** For details of the customized site-specific polyclonal antibody to OGG1 pS326 (Anti-p-OGG1S326) as well as commercially purchased antibodies, see *SI Appendix, Materials and Methods*.

***Cell culture and treatment.*** $Ogg1^{+/+}$, $Ogg1^{-/-}$ MEF cells, HeLa cells (ATCC, Cat# CL-0101) and HEK293 (ATCC, Cat# ORC0001) cells were grown in high glucose DMEM (Gibco REF# 12800017) supplemented with 10% fetal bovine serum. For the details of cell treatment, see *SI Appendix, Materials and Methods*.

***Animals.*** Animal use, treatment, and euthanasia are in accordance with the Environmental and Facilities for Laboratory Animals (GB14925-2010) and the Guidelines for Ethical Review of Welfare of Laboratory Animals (GB/T 35892-2018), and approved by the local ethics committee (reference number:202302205, the institutional animal care and use committee (IACUC) of the Northeast Normal University). For details, see *SI Appendix, Materials and Methods*.

***Acute lung injury model.*** Acute lung injury model was set up as described previously (26). For details, see *SI Appendix, Materials and Methods*.

***Plasmids and transfection.*** The details of the eukaryotic and prokaryotic expression plasmids' construction were described in *SI Appendix, Materials and Methods*. All the plasmids were transfected using Lipofectamine 3000 reagent (Invitrogen, Cat# L3000008 Carlsbad, CA) according to the manufacturer's instructions.

***siRNA mediated gene silencing.*** For RNA interference experiments, scramble control, or siRNA targeting CDK4 were transfected into HEK293 cells using Lipofectamine 3000 according to the manufacturer's instructions. For details, see *SI Appendix, Materials and Methods*.

***Reverse transcription and RT-qPCR.*** Total RNA was isolated from cultured cells using TRIzol reagent (TIANGEN, Cat#DP421). The details of reverse transcription and real-time quantitative PCR (RT-qPCR) were described in *SI Appendix, Materials and Methods*.

***Co-Immunoprecipitation and western-blotting.*** Co-Immunoprecipitation and western-blotting were performed as previously described (24). For details, see *SI Appendix, Materials and Methods*.

***Peptide dot-blot.*** Peptide dot blots were used to test the specificity of Anti-pan-OGG1S326 antibody. For details, see *SI Appendix, Materials and Methods*.

***PLA.*** HeLa cells grown on collagen treated coverslip slides were fixed with 4% paraformaldehyde, and then permeabilized with 0.1% (w/v) of Triton X-100 diluted in phosphate-buffered saline (PBST) for 5 min. In selected experiments cells were fractionated in situ using cytoskeletal (CSK) buffer (61). PLA was performed using the Duolink PLA kit (OLink Biosci-ence Cat# LNK-92101-KI01) as we described previously (24). For details, see *SI Appendix, Materials and Methods*.

***GST-fused protein purification.*** GST and GST-fused proteins were produced in BL21 of *Escherichia coli*. The details of GST-fused protein purification were describe in *SI Appendix, Materials and Methods*.

***High phosphate recombinant protein assay.*** The compatible expression system for the production of highly phosphorylated recombinant protein in *E. coli* was set up. For details, see *SI Appendix, Materials and Methods*.

***In vitro kinase assay.*** Recombinant His-CDK4 (20 μg/mL) purified bacterially was incubated with recombinant GST-OGG1 (20 ug/mL) in phosphorylation reaction buffer. The details of In vitro kinase assay were described in *SI Appendix, Materials and Methods*.

***LC-MS/MS analysis of OGG1 phosphorylation.*** An in vitro kinase reaction was set up by incubating recombinant proteins His-CDK4 and GST-OGG1 in the presence of ATP, and then subjected to SDS-PAGE. LC-MS analysis of OGG1 phosphorylation was performed. For the details, see *SI Appendix, Materials and Methods*. The mass spectrometry proteomics data of OGG1 phosphorylation have been deposited to the ProteomeXchange Consortium via the PRIDEpartner repository (62, 63).

***EMSA.*** The oligonucleotides were synthesized by Sangon Biotech (Shanghai, China), and the site specific-guanine residue within each of the oligonucleotides was modified with a single 8-oxoGua. The details of electrophoretic mobility shift assay (EMSA) were described in *SI Appendix, Materials and Methods*.

***Oligonucleotide incision (cleavage) assay.*** To examine the lesion incision abilities of wt-OGG1 and OGG1 mutants, a 37-mer oligonucleotide containing an 8-oxoGua at position 16 and labeled at the 3′ end with Cy5 was used. For the details of incision assay, see *SI Appendix, Materials and Methods*.

***ChIP.*** Chromatin immunoprecipitation (ChIP) was performed as previously described (24). For details, see *SI Appendix, Materials and Methods*.

***RNA fluorescence in situ hybridization.*** $Ogg1^{-/-}$ MEF cells grown on a glass coverslip were transfected with YFP, YFP-OGG1, YFP-OGG1S326C or YFP-OGG1F319A plasmids. After TNFα addiction for increasing lengths of time, cells were fixed with 4% of paraformaldehyde (Dingguo, China) for 10 min at room temperature, permeabilized with 0.5% (v/v) of Triton X-100 for 30 min. The details of EMSA were described in *SI Appendix, Materials and Methods*.

***FLARE Comet assay.*** Genomic 8-oxoGua levels were determined by assessing OGG1-sensitive sites using a FLARE™ comet assay kit (Trevigen, Gaithersburg, MD). The details of Fragment Length Analysis using Repair Enzymes (FLARE) Comet assay were described in *SI Appendix, Materials and Methods*.

***Confocal imaging and FRET acceptor photobleaching technique.*** Confocal imaging and Fluorescence Resonance Energy Transfer (FRET) analysis were performed on a confocal microscope (LS/M510/ConfoCor2, Zeiss, Jena, Germany). HeLa cells were co-transfected with donor CFP-wt-OGG1 and acceptor YFP-wt-OGG1, or donor CFP-OGG1S326C and acceptor YFP-OGG1S326C. As a positive control, fused CFP-YFP protein was used to show the occurrence of FRET. FRET analysis was performed as described previously (64). For details, see *SI Appendix, Materials and Methods*.

***Evaluation of airway inflammation.*** Inflammatory responses in the airways following challenge were examined as we described previously (21). For details of broncho-alveolar lavage fluids (BALF) and histological analyses, see *SI Appendix, Materials and Methods*.

**Data, Materials, and Software Availability.** Mass Spectrometry data have been deposited in Pride (PXD059565) (36). All study data are included in the article and/or *SI Appendix*.

**ACKNOWLEDGMENTS.** This work was supported by the following grants: National Natural Science Foundation of China (32170591, 31970686), Provincial

Science Foundation of Jilin, China (20220203147SF), Scientific research project of Jilin Provincial Department of Education (JJKH20250323KJ), United States National Institute of Allergic and Infectious Diseases AI062885.

Author affiliations: [a]Division of Human Health, Key Laboratory of Molecular Epigenetics of Ministry of Education, Northeast Normal University, Changchun 130024, China; [b]Division of Cell Biology, School of Life Sciences, Northeast Normal University, Changchun 130024, China; [c]Department of Respiratory Medicine, China-Japan Union Hospital of Jilin University, Changchun 130061, China; [d]Lung Transplant Center, Department of Respiratory Medicine, The Affiliated Wuxi People's Hospital of Nanjing Medical University, Wuxi People's Hospital, Wuxi Medical Center, Nanjing Medical University, Wuxi, Jiangsu 214023, China; [e]Research Center for Molecular Exercise Science, Institute of Sport Science, University of Physical Education, Budapest H-1123, Hungary; [f]Division of Neurofunctional Genomics, Department of Immunobiology and Neuroscience, Medical Institute of Bioregulation, Kyushu University, Fukuoka 812-8582, Japan; and [g]Department of Microbiology and Immunology, University of Texas Medical Branch at Galveston, Galveston, TX 77555


1. U. S. Srinivas, B. W. Q. Tan, B. A. Vellayappan, A. D. Jeyasekharan, ROS and the DNA damage response in cancer. *Redox Biol.* **25**, 101084 (2019).
2. R. Wang, W. Hao, L. Pan, I. Boldogh, X. Ba, The roles of base excision repair enzyme OGG1 in gene expression. *Cellular Mol. Life Sci.: CMLS* **75**, 3741–3750 (2018).
3. C. J. Burrows, J. G. Muller, Oxidative nucleobase modifications leading to strand scission. *Chem. Rev.* **98**, 1109–1152 (1998).
4. X. Ba, I. Boldogh, 8-Oxoguanine DNA glycosylase 1: Beyond repair of the oxidatively modified base lesions. *Redox Biol.* **14**, 669–678 (2018).
5. Z. Radak, I. Boldogh, 8-Oxo-7,8-dihydroguanine: Links to gene expression, aging, and defense against oxidative stress. *Free Radical Biol. Med.* **49**, 587–596 (2010).
6. T. Kohno *et al.*, Genetic polymorphisms and alternative splicing of the hOGG1 gene, that is involved in the repair of 8-hydroxyguanine in damaged DNA. *Oncogene* **16**, 3219–3225 (1998).
7. K. Janssen *et al.*, DNA repair activity of 8-oxoguanine DNA glycosylase 1 (OGG1) in human lymphocytes is not dependent on genetic polymorphism Ser326/Cys326. *Mutation Res.* **486**, 207–216 (2001).
8. R. J. Hung, J. Hall, P. Brennan, P. Boffetta, Genetic polymorphisms in the base excision repair pathway and cancer risk: A HuGE review. *Am. J. Epidemiol.* **162**, 925–942 (2005).
9. T. Kohno *et al.*, Association of the OGG1-Ser326Cys polymorphism with lung adenocarcinoma risk. *Cancer Sci.* **97**, 724–728 (2006).
10. F. Farinati *et al.*, Oxidative DNA damage in gastric cancer: CagA status and OGG1 gene polymorphism. *Int. J. Cancer* **123**, 51–55 (2008).
11. L. Chen, A. Elahi, J. Pow-Sang, P. Lazarus, J. Park, Association between polymorphism of human oxoguanine glycosylase 1 and risk of prostate cancer. *J. Urol.* **170**, 2471–2474 (2003).
12. A. Elahi *et al.*, The human OGG1 DNA repair enzyme and its association with orolaryngeal cancer risk. *Carcinogenesis* **23**, 1229–1234 (2002).
13. F. Thameem *et al.*, The Ser(326)Cys polymorphism of 8-oxoguanine glycosylase 1 (OGG1) is associated with type 2 diabetes in Mexican Americans. *Hum. Heredity* **70**, 97–101 (2010).
14. Y. Dinçer *et al.*, DNA repair gene OGG1 polymorphism and its relation with oxidative DNA damage in patients with Alzheimer's disease. *Neurosci. Lett.* **709**, 134362 (2019).
15. A. L. da Silva *et al.*, Evaluation of DNA damage in COPD patients and its correlation with polymorphisms in repair genes. *BMC Med. Genetics* **14**, 93 (2013).
16. J. Morreall *et al.*, Inactivation of a common OGG1 variant by TNF-alpha in mammalian cells. *DNA Repair* **26**, 15–22 (2015).
17. C. Dherin, J. P. Radicella, M. Dizdaroglu, S. Boiteux, Excision of oxidatively damaged DNA bases by the human alpha-hOgg1 protein and the polymorphic alpha-hOgg1(Ser326Cys) protein which is frequently found in human populations. *Nucleic Acids Res.* **27**, 4001–4007 (1999).
18. R. A. Mateuca *et al.*, hOGG1(326), XRCC1(399) and XRCC3(241) polymorphisms influence micronucleus frequencies in human lymphocytes in vivo. *Mutagenesis* **23**, 35–41 (2008).
19. L. Pan *et al.*, Oxidized Guanine Base Lesions Function in 8-Oxoguanine DNA Glycosylase-1-mediated Epigenetic Regulation of Nuclear Factor κB-driven Gene Expression. *J. Biol. Chem.* **291**, 25553–25566 (2016).
20. W. Hao *et al.*, Enzymatically inactive OGG1 binds to DNA and steers base excision repair toward gene transcription. *FASEB J.* **34**, 7427–7441 (2020).
21. X. Zheng *et al.*, innate immune responses to RSV infection facilitated by OGG1, an Enzyme repairing oxidatively modified DNA base lesions. *J. Innate Immunity* **14**, 593–614 (2022).
22. X. Ba *et al.*, The role of 8-oxoguanine DNA glycosylase-1 in inflammation. *Int. J. Mol. Sci.* **15**, 16975–16997 (2014).
23. W. Hao *et al.*, Effects of the stimuli-dependent enrichment of 8-oxoguanine DNA glycosylase1 on chromatinized DNA. *Redox Biol.* **18**, 43–53 (2018).
24. Y. Xue *et al.*, 8-Oxoguanine DNA glycosylase 1 selectively modulates ROS-responsive NF-κB targets through recruitment of MSK1 and phosphorylation of RelA/p65 at Ser276. *J. Biol. Chem.* **299**, 105308 (2023).
25. H. Sugimura *et al.*, hOGG1 Ser326Cys polymorphism and lung cancer susceptibility. *Cancer Epidemiol. Biomarkers Prev.* **8**, 669–674 (1999).
26. T. Visnes *et al.*, Small-molecule inhibitor of OGG1 suppresses proinflammatory gene expression and inflammation. *Science (New York, N.Y.)* **362**, 834–839 (2018).
27. O. D'Augustin *et al.*, Identification of key residues of the DNA glycosylase OGG1 controlling efficient DNA sampling and recruitment to oxidized bases in living cells. *Nucleic Acids Res.* **51**, 4942–4958 (2023).
28. P. A. van der Kemp, J. B. Charbonnier, M. Audebert, S. Boiteux, Catalytic and DNA-binding properties of the human Ogg1 DNA N-glycosylase/AP lyase: Biochemical exploration of H270, Q315 and F319, three amino acids of the 8-oxoguanine-binding pocket. *Nucleic Acids Res.* **32**, 570–578 (2004).
29. J. W. Hill, M. K. Evans, Dimerization and opposite base-dependent catalytic impairment of polymorphic S326C OGG1 glycosylase. *Nucleic Acids Res.* **34**, 1620–1632 (2006).
30. T. Paz-Elizur *et al.*, DNA repair of oxidative DNA damage in human carcinogenesis: Potential application for cancer risk assessment and prevention. *Cancer Lett.* **266**, 60–72 (2008).
31. H. Sampath, R. S. Lloyd, Roles of OGG1 in transcriptional regulation and maintenance of metabolic homeostasis. *DNA Repair* **81**, 102667 (2019).
32. F. Dantzer, L. Luna, M. Bjørås, E. Seeberg, Human OGG1 undergoes serine phosphorylation and associates with the nuclear matrix and mitotic chromatin in vivo. *Nucleic Acids Res.* **30**, 2349–2357 (2002).
33. J. Hu, S. Z. Imam, K. Hashiguchi, N. C. de Souza-Pinto, V. A. Bohr, Phosphorylation of human oxoguanine DNA glycosylase (alpha-OGG1) modulates its function. *Nucleic Acids Res.* **33**, 3271–3282 (2005).
34. D. Tempka *et al.*, Downregulation of PARP1 transcription by CDK4/6 inhibitors sensitizes human lung cancer cells to anticancer drug-induced death by impairing OGG1-dependent base excision repair. *Redox Biol.* **15**, 316–326 (2018).
35. L. Luna *et al.*, Dynamic relocalization of hOGG1 during the cell cycle is disrupted in cells harbouring the hOGG1-Cys326 polymorphic variant. *Nucleic Acids Res.* **33**, 1813–1824 (2005).
36. J. Han *et al.*, Assessment of CDK4 as a serine kinase phosphorylating OGG1. PRIDE. https://www.ebi.ac.uk/pride/archive/projects/PXD059566. Deposited 18 April 2025.
37. S. S. David, V. L. O'Shea, S. Kundu, Base-excision repair of oxidative DNA damage. *Nature* **447**, 941–950 (2007).
38. A. Bravard *et al.*, Oxidation status of human OGG1-S326C polymorphic variant determines cellular DNA repair capacity. *Cancer Res.* **69**, 3642–3649 (2009).
39. J. I. Kim *et al.*, hOGG1 Ser326Cys polymorphism modifies the significance of the environmental risk factor for colon cancer. *World J. Gastroenterol.* **9**, 956–960 (2003).
40. N. S. Aslan, G. Orhan, B. Karahalil, The impacts of prominent gene polymorphisms in DNA repair enzymes on Parkinson's disease. *Neurosci. Lett.* **735**, 135203 (2020).
41. V. S. Sidorenko, A. P. Grollman, P. Jaruga, M. Dizdaroglu, D. O. Zharkov, Substrate specificity and excision kinetics of natural polymorphic variants and phosphomimetic mutants of human 8-oxoguanine-DNA glycosylase. *The FEBS J.* **276**, 5149–5162 (2009).
42. M. P. Kaur *et al.*, Cellular accumulation of Cys326-OGG1 protein complexes under conditions of oxidative stress. *Biochem. Biophys. Res. Commun.* **447**, 12–18 (2014).
43. N. Blom, S. Gammeltoft, S. Brunak, Sequence and structure-based prediction of eukaryotic protein phosphorylation sites. *J. Mol. Biol.* **294**, 1351–1362 (1999).
44. O. G. Berg, R. B. Winter, P. H. von Hippel, Diffusion-driven mechanisms of protein translocation on nucleic acids. 1. Models and theory. *Biochemistry* **20**, 6929–6948 (1981).
45. M. Slutsky, L. A. Mirny, Kinetics of protein-DNA interaction: Facilitated target location in sequence-dependent potential. *Biophys. J.* **87**, 4021–4035 (2004).
46. L. Cintori, A. M. Di Guilmi, Y. Canitrot, S. Huet, A. Campalans, Spatio-temporal dynamics of the DNA glycosylase OGG1 in finding and processing 8-oxoguanine. *DNA Repair* **129**, 103550 (2023).
47. T. Hu, B. I. Shklovskii, How a protein searches for its specific site on DNA: The role of intersegment transfer. *Phys. Rev. E Stat. Nonlinear Soft Matter. Phys.* **76**, 051909 (2007).
48. M. A. Schaich *et al.*, Single-molecule analysis of DNA-binding proteins from nuclear extracts (SMADNE). *Nucleic Acids Res.* **51**, e39 (2023).
49. P. C. Blainey, A. M. van Oijen, A. Banerjee, G. L. Verdine, X. S. Xie, A base-excision DNA-repair protein finds intrahelical lesion bases by fast sliding in contact with DNA. *Proc. Natl. Acad. Sci. U.S.A.* **103**, 5752–5757 (2006).
50. M. A. Schaich, T. M. Weaver, V. Roginskaya, B. D. Freudenthal, B. Van Houten, Single-molecule analysis of purified proteins and nuclear extracts: Insights from 8-oxoguanine glycosylase 1. *DNA Repair* **134**, 103625 (2024).
51. D. Li *et al.*, Small cell lung cancer (SCLC) incidence and trends vary by gender, geography, age, and subcategory based on population and hospital cancer registries in Hebei, China (2008–2017). *Thoracic Cancer* **11**, 2087–2093 (2020).
52. L. Maiorino, J. Daßler-Plenker, L. Sun, M. Egeblad, Innate Immunity and Cancer Pathophysiology. *Annu. Rev. Pathol.* **17**, 425–457 (2022).
53. H. Zhao *et al.*, Inflammation and tumor progression: Signaling pathways and targeted intervention. *Signal Trans. Targeted Ther.* **6**, 263 (2021).
54. H. Shi *et al.*, Chemokine (C-X-C motif) ligand 1 and CXCL2 produced by tumor promote the generation of monocytic myeloid-derived suppressor cells. *Cancer Sci.* **109**, 3826–3839 (2018).
55. X. Han *et al.*, Correction: CXCR2 expression on granulocyte and macrophage progenitors under tumor conditions contributes to mo-MDSC generation via SAP18/ERK/STAT3. *Cell Death Disease* **10**, 641 (2019).
56. H. Simon *et al.*, OGG1 deficiency alters the intestinal microbiome and increases intestinal inflammation in a mouse model. *PloS One* **15**, e0227501 (2020).
57. H. Sampath *et al.*, 8-Oxoguanine DNA glycosylase (OGG1) deficiency increases susceptibility to obesity and metabolic dysfunction. *PloS One* **7**, e51697 (2012).
58. M. Schatz, S. H. Sicherer, D. A. Khan, R. S. Zeiger, The journal of allergy and clinical immunology: In practice 2019 highlights. *J. Allergy Clin. Immunol. In Practice* **8**, 912–936 (2020).
59. J. W. Windsor, G. G. Kaplan, Evolving epidemiology of IBD. *Current Gastroenterol. Rep.* **21**, 40 (2019).
60. Y. K. Tahara *et al.*, Potent and selective inhibitors of 8-oxoguanine DNA glycosylase. *J. Am. Chem. Soc.* **140**, 2105–2114 (2018).
61. A. Sawasdichai, H. T. Chen, N. Abdul Hamid, P. S. Jayaraman, K. Gaston, In situ subcellular fractionation of adherent and non-adherent mammalian cells. *J. Vis. Exp.: JoVE* **41**, 1958 (2010).
62. Y. Perez-Riverol *et al.*, The PRIDE database at 20 years: 2025 update. *Nucleic Acids Res.* **53**, D543–d553 (2025).
63. E. W. Deutsch *et al.*, The ProteomeXchange consortium at 10 years: 2023 update. *Nucleic Acids Res.* **51**, D1539–D1548 (2023).
64. Y. Y. Lu, T. S. Chen X, P. Wang L. Li, Single-cell analysis of dihydroartemisinin-induced apoptosis through reactive oxygen species-mediated caspase-8 activation and mitochondrial pathway in ASTC-a-1 cells using fluorescence imaging techniques. *J. Biomed. Optics* **15**, 046028 (2010).